ENTANGLEMENT SWELLING IN POLYMER GLASSES

ENTANGLEMENT SWELLING IN POLYMER GLASSES: CHAIN LENGTH DEPENDENCE ON PARTICIPATION IN NETWORK EVENTS

By

JOSHUA D. MCGRAW, B.Sc.

A Thesis
Submitted to the School of Graduate Studies
in Partial Fulfillment of the Requirements
for the Degree
Master of Science

McMaster University

MASTER OF SCIENCE (2008)
(Physics)

McMaster University
Hamilton, Ontario

TITLE: Entanglement swelling in polymer glasses: Chain length dependence on participation in network events

AUTHOR: Joshua D. McGraw, B.Sc.(Dalhousie University)

SUPERVISOR: Dr. Kari Dalnoki-Veress

NUMBER OF PAGES: viii, 64

Abstract

When a polymer system is strained below its glass transition temperature, T_g, deformed regions called crazes may be formed that have a characteristic extension ratio, λ. Examining the regions of deformed material, which are almost visible to the naked eye, and measuring λ with the use of atomic force microscopy gives information about the space between entanglements along a polymer chain, which is a truly molecular quantity. In this work we present the results of experiments in which entanglements in high molecular weight polystyrene (PS) samples have effectively been swelled by diluting the network with low molecular weight PS. We find that these experiments not only tell us how the molecular weight of a polymer can affect its contribution to the polymer network, but also give an entirely new method of determining the entanglement molecular weight, M_e, of a polymer system.

Acknowledgements

To start it off, my lab mates ought to be acknowledged for being cowboys and Yanks, roosters, one and a half *fleur de lis* and a stallion. Thanks for the cartoons and never failing to point out my knobbery, you've all taught me a thing or two in the lab as well. Undergrads have at times made me feel smart, even if my suggestions never amounted to a single extra data point.

To friends old and new, thanks for giving me something to go to when the n^{th} bag broke and I just couldn't hack it any more. Thanks for not making me go to the Casbah alone and for the useful discussions.

Thanks Mom and Dad for getting me here. Life's been different in the Hammer, but it's great to know that you and the gang are there whenever the mood and the means strike. Thanks, Dad, for the support you gave me just before the March meeting.

Kari, this introduction to polymers has been very exciting. Thanks for knowing when to let me stray, but also knowing when to keep the leash tight. You've been a wonderful teacher in the lab, and in all things science for that matter.

Were it the case that my time here was up following this submission, I could emphatically say that my life was richer. As it happens, I'm looking forward to the next bit.

Contents

List of Figures

Chapter 1

Preliminaries

When a polymer system is strained below its glass transition temperature, T_g, microscopic crack-like defects called crazes may be formed. Like cracks, craze formation is the result of energy dissipation in the creation of newly exposed surface atoms. However, where cracks are void of the strained material, crazes are composed of an interconnected fibrillar structure bridging a gap between undeformed material. Much attention has been paid to the structure of crazes and the dynamics their formation through the last few decades as their properties are responsible for what is macroscopically seen as the failure of a polymer glass. Many of the previous studies have been focused on understanding the microscopic processes that govern the nucleation [1], growth [2, 3] and breakdown [3] of these defects as the strain increases. Drawing on the results of these studies, it has been seen that one may compare the strained and unstrained material in a crazed specimen to learn about how polymers are arranged in confined geometries [4].

In this work we continue the use of crazing experiments. Here however, we do not use crazing for the purposes of studying what happens to a polymer glass when it is subjected to strain, as has been done so well in the past. On the contrary, we use crazing as a tool to learn more about how polymer molecules are arranged in systems that are *undeformed.* At the outset, the question we wished to answer was the following: what happens to a polymer network when one systematically 'removes' a given number of entanglements? To effectively remove entanglements from one system to the next, we swell the polymer network which results in fewer entanglements per unit volume. The method by which entanglements are removed or swelled led to a new question: how does the length of a polymer chain affect its ability to participate in phenomena which occur as a result of the polymer chains being entangled? While answering this question, we found that the analysis of the experimental results presented herein led to an entirely new method of determining the entanglement molecular weight, M_e, of a polymer species.

In this chapter, the concept of entanglement molecular weight will be discussed and a fairly lengthy description of the standard method of its measurement will be presented. This topic naturally leads to an explanation of the entropy of a Gaussian polymer chain and a section concerning the viscoelastic behaviour of polymers. The process of crazing from nucleation to failure is also discussed, with emphasis on the process by which a craze grows. Less attention will be given to craze nucleation and craze breakdown as these topics do not directly concern the results which will be presented later.

Requisite concepts

I Entanglements

In a polymer melt, a given chain samples a large number of possible configurations which may lead it to become tangled with many of the other chains in the space around it. The interactions between two chains which restrict motion perpendicular to the chain backbone are known as entanglements. A schematic of the basic idea behind entanglement is shown in Figure 1.1. The figure depicts what should be considered as segments from three different polymer molecules that are representative of the rest of the network. Since the two polymer molecules that are arranged vertically are uncrossable, the mobility of the lateral molecule is significantly reduced. One can take the knots in Figure 1.1 to be fixed so that the lateral polymer passing through them is only allowed to move like a worm through the knots that encompass it. The worm-like motion of a polymer chain has been called 'reptation' [5]. This type of motion is to be contrasted to that of an ideal gas molecule which is uninhibited by all of the other molecules in the system and is constrained only by the walls of its container.

On an elementary level, entanglements can be thought of as one polymer chain knotted around another. The precise chain-chain configurations defining an entanglement are not known, but the notion of one polymer chain completely wrapping around another is a rather extreme condition for two chains to be entangled. There are statistical ideas that have proven to be useful [6, 7], one of which is summarized in the next section. The basic idea [6], which has been experimentally verified, states that a system of chains wherein each chain shares its pervaded volume, V_p, with at least a few other chains can be considered to be entangled. V_p is defined as the volume swept out by a sphere whose diameter is proportional to the distance spanned by the ends of a polymer chain (the end-to-end distance, R).

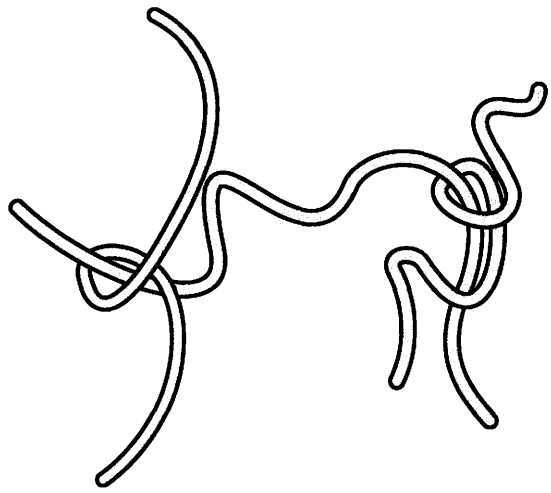

Figure 1.1: Schematic of two entanglements on a polymer chain. The 'entanglement molecular weight', M_e is the mass of material between the two loops. The loops represent the interactions that produce entanglement effects.

II A description of M_e

In this thesis the concept of entanglement molecular weight M_e and its pseudonyms are discussed at length. The terms *entanglement molecular weight*, *entanglement length*, *entanglement strand*, and *entanglement density* are referred to often and somewhat interchangeably, but they all refer to essentially the same concept. In a system of polymers there are what might be considered knots, or entanglements between the chains that greatly restrict the motion of the molecules because one polymer chain cannot cross another one. For a given polymer system, one can define an average spacing between the knots and it turns out that a natural variable that is used to describe this distance is the molecular weight of a segment between the knots, this is what we refer to as M_e, the *entanglement molecular weight.*

It can be shown that in a melt of polymer chains any given chain undergoes a random walk between its ends [8]. As a result of this, the mean-square end-to-end distance $\langle R^2 \rangle$ of a polymer segment [1] with molecular weight M is given by

$$\langle R^2 \rangle = \beta M. \tag{1.1}$$

β is a constant for a given type of polymer, for example if the polymer is polystyrene (PS) then $\beta = 0.08$ Å^2 mol/g [9]. It will come up later in this thesis, but its numerical value will never need to be considered [2] . The distance spanned by a segment of chain whose molecular

[1]The term 'segment' is used deliberately in place of the term 'chain' here. This is because the random walk concept applies not only to entire chains, but also more generally to any *part* of a chain, down to some minimum segment size.

[2]β can be measured by labeling small concentrations of chains in a polymer glass with neutrons and

weight is that of the average between entanglements, M_e, is then $\langle R_e^2 \rangle = \beta M_e$ and this is what is referred to as the *entanglement length.* An *entanglement strand* is just any segment of chain whose molecular weight is M_e. The usefulness of the concept of M_e will come when we try to explain the results of our experiments in terms of molecular quantities.

The fourth important quantity is the *entanglement density,* ν_e. As its name suggests, it measures the number of knots per unit volume and will be a useful quantity in modeling the systems we study here. The relation between M_e and ν_e is rather simple, $M_e \sim 1/\nu_e$. This can be understood by considering Figure 1.1: if there are a lot of monomers between entanglements, then M_e is large. Given that there many monomers between the entanglements, they must be far apart and thus ν_e is comparatively small.

i Why M_e has a well defined average

To understand what factors control M_e consider the following analogy. Holding a length of shoelace about a metre in length, if one tries to tie a knot in said string (say, a bowline) it is found that the knot is easily tied. It is also possible to start with a length of string which is half as long and demand that the same knot be tied, probably the task can still be accomplished at this stage. Cutting the string in half and attempting to tie the knot can only be iterated so many times though; at a certain point it will be found that the string simply isn't long or flexible enough to tie the desired knot. Given this analogy, it is easy to see that the chains which make up a monodisperse system of polymers must have some minimum length to entangle. In terms of polymer chains, we can say that there is an energy cost associated with trying to bend a polymer chain too tightly around itself or another chain, giving further reason to require a minimum entanglement length.

Now consider a system [3] of 1 trillion lengths of string. If entropy dominates this system, then the ropes will not be an ordered pile of cylinders, as might be found on the bed of a logging truck. This is because there are relatively few string configurations that look like ordered, stacked cylinders. On the other extreme, there are also relatively few configurations which lead the chains to become so entangled that there are only a couple of string widths between knots, or, that would cause the strings to bunch up into individual balls of yarn. Hence, entropy chooses a string configuration in which the chains have knots that are spaced not too far apart and a combination of entropy, geometry or topology, and energy forces the

performing neutron scattering experiments. The scattering profile is related to the size of a chain, so scattering experiments with a range of M gives $\beta/6$ as the slope of a plot of $\langle R^2 \rangle$ vs. M. The factor of 6 comes from the fact that scattering experiments don't measure the end-to-end distance of a polymer chain, they measure the so-called radius of gyration, which is the average distance of a given monomer from the center of mass of the chain.

[3] To make the analogy commensurate with our experiments, recognize that the systems we study are approximately 1.5 mm × 5 mm × 130 nm in size and that the density and molecular weight of PS used here are 1050 kg/m^3 and 785 kg/mol respectively. Given these numbers, one can calculate that the systems we study contain roughly 10^{12} polymer chains

system to separate the knots by some minimum distance.

The concept that chains must have some minimum length to entangle has been experimentally observed as a change in scaling behaviour of viscosity as a function of molecular weight. Below the minimum molecular weight, the viscosity of a melt of polymer chains scales like $\eta \sim M$ while after the onset of entanglement it scales like $\eta \sim M^{3.4}$ [10]. This is a way in which one can find M_e for a given polymer species: measure the viscosity for a series of systems in which the constituent chains' M is varied. A kink in the graph of η vs. M is a molecular weight which can be related [7] to M_e.

ii The entanglement onset of Fetters

The argument for the onset of entanglement due to Fetters *et al.*[6], which makes no reference to the actual shape or trajectory of any specific polymer chain, will now be summarized. The idea behind the model is that a longer chain will sweep out a larger volume. If the volume a chain sweeps out is large, then it will have a higher probability of interacting with other chains around it, hence entanglement occurs more often for longer chains. The pervaded volume of a given test chain is

$$V_p = A\langle R^2\rangle^{\frac{3}{2}}, \tag{1.2}$$

where A is a constant of order unity and $\langle R^2\rangle$ is the mean square end-to-end distance of the chain. V_p is shown as the grey circle of Figure 1.2 and the test chain is the white one in the same figure. The volume that the chain actually occupies though, is smaller than V_p and is just given by $V_c = M/\rho N_A$ where ρ is the material density and N_A is Avogadro's number. If N is the number of chains that would occupy V_p, that is $N = V_p/V_c$, then from Equations 1.1 and 1.2 we have

$$N = \frac{A\,(\beta M)^{\frac{3}{2}}}{M/\rho N_A}. \tag{1.3}$$

Now consider V_p for a single test chain, P. In this volume there will be some number of chain segments. If m_1 is the molecular weight of a single monomer, then M/m_1 of the monomers in V_p belong to P. The rest of V_p is filled by chain segments (or monomers) that belong to other chains randomly walking into V_p, as shown in Figure 1.2(a); the molecular weight of all the segments in V_p that don't belong to P should be the same as a chain with molecular weight $(N-1)\,M$. A schematic of this idea is shown in Figure 1.2(b).

Fetters suggests that entanglement occurs when some prescribed value of N is reached: $N = N_e$. Here $N_e > 1$ but of order unity. Fetters prescribes $N_e = 2$ and states that for this

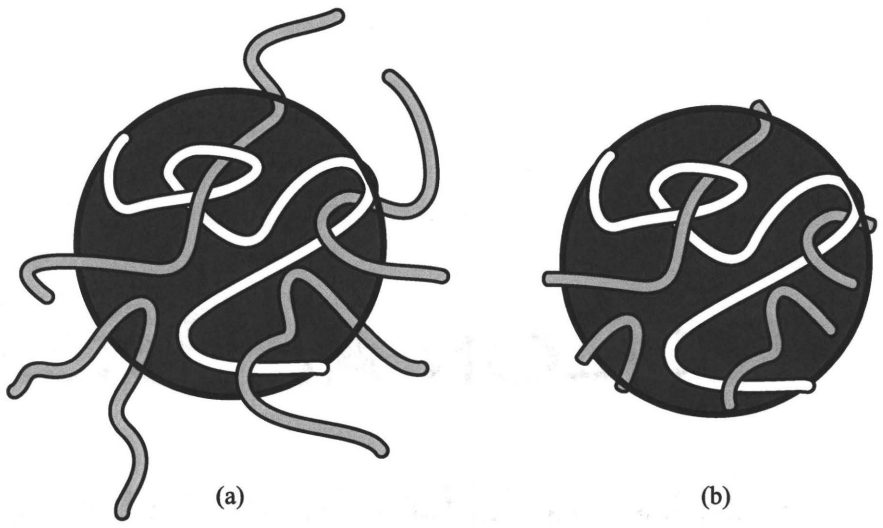

Figure 1.2: (a) The pervaded volume of the test chain (white) and all of the other (grey) chains that enter V_p. (b) shows all of the chain segments of the chains that have entered V_p. These are the segments that contribute to the (white) test chain's entanglement.

specific value of N, $M = M_e$. Given this conjecture we get from Equation 1.3

$$M_e = \frac{1}{\beta^3}\left(\frac{N_e}{A\rho N_A}\right)^2. \tag{1.4}$$

With the exception of N_e, all of the quantities on the right hand side of Equation 1.4 are known parameters, so this gives a theoretically predicted value of M_e. *If* one calls M_e the molecular weight at which there is a change in viscosity scaling (as was briefly described at the end of the previous section), then Equation 1.4 can be compared to the experimental value to see what value of N_e defines M_e in this case. This molecular weight is given a different special name, M_c, and M_e is defined as the molecular weight determined from the plateau modulus (to be discussed below, see Equation 1.13). There seems to be some consensus [11] that $M_c = 2M_e$ but the universality of this claim is doubted [7]. Typically M_e is defined in a considerably different manner which will be described following a diversion into the viscoelasticity of polymers.

III Stretching and straining liquid and rubbery polymer systems

A rubber band is a material composed of polymer molecules whose relative positions are fixed in space; they are not allowed to reptate past one another. While entanglements

are the result of nonpermanent interactions between two different chains who share the same pervaded volume, it is possible to induce a permanent connection between chains by chemically bonding them together, this is known as cross-linking. A rubber band is a material in which many of the entanglements in the system can be thought to have been converted into permanently connected cross-links. The system is essentially one giant molecule by virtue of the fact that any one chain segment can be accessed by following a path along other segments in the system. If the temperature is high enough the system may be deformed uniformly by the application of tension to both of its ends. If tension is applied to a rubber band, it stretches by some amount. In a system for which there are no cross-links, the entanglements would relax and the individual molecules would reptate past one another, this is not possible for a rubber band (as long as the tension is not to large) because the cross-links are permanent connections.

In this situation, the energy that has gone into stretching the rubber band is stored in the polymer molecules as a result of their being elongated. Unlike the typical $f = -kx$ spring encountered in many first year mechanics courses, whose energy storage is due to displacement of atoms from their potential *energy* equilibrium positions, polymer molecules' spring forces are entropic in origin. Surprisingly though, the force law for the elongation of a polymer chain indeed turns out to be linear in the stretching distance as will be shown now.

We first need to calculate the entropy for a single polymer chain. Using the entropy, which will turn out to be quadratic in the end-to-end distance R, we will be able to write down the free energy. If the free energy is quadratic in R, then the force on a chain is linear in R since the force, f is related to the free energy, F, by $f = \frac{dF}{dR}$. While the force required to stretch a single chain is linear, we will see that the force required to deform a network of polymer chains is not so simple. In that case, the force required to stretch a network of polymer chains (a rubber band, for example) will end up with a non linear term, as will be shown below. For a more complete description, and for the inspiration to the arguments that follow, see the books by Rubenstein and Colby [12] and also by Jones [13].

i The entropy and free energy of a single polymer chain

Polymer chains' trajectories are random walks and as a result the probability density function of an ensemble of chains' end-to-end distances is given by a Gaussian distribution, $\rho(R) = Ce^{-\alpha R^2}$ where C is a normalization constant and α is also a constant. Normalizing over 3-space, $\int \rho(R) d^3r = 1$ we find that $C = \left(\frac{\alpha}{\pi}\right)^{\frac{3}{2}}$. Equation 1.1 gives the mean square end-to-end distance of a polymer chain, but we can also calculate it by integrating $R^2\rho(R)$ over all space to find $\langle R^2 \rangle = 3/2\alpha$. Using this and Equation 1.1 we can write the probability density function for the size of an *ideal* polymer chain in terms of the molecular weight, M

and the material parameter β as

$$\rho(R) = \left(\frac{3}{2\pi\beta M}\right)^{\frac{3}{2}} \exp\left(\frac{-3R^2}{2\beta M}\right). \tag{1.5}$$

The entropy S is given by the classic Boltzmann equation

$$S = k\ln(\Omega(R)), \tag{1.6}$$

where k is the Boltzmann constant and $\Omega(R)$ is the number of random walks that give an end-to-end distance R. The probability that a chain has R for the end-to-end distance is just the number of walks that give R, $\Omega(R)$, divided by the total number of distinct walks available to the chain, $\int \Omega(R)d^3r$, or

$$\rho(R) = \frac{\Omega(R)}{\int \Omega(R)d^3r}. \tag{1.7}$$

Then, to write the entropy of a single polymer chain for a given R, we need only know the probability density function and the total number of walks available to the chain since $\Omega(R) = \rho(R)\int \Omega(R)d^3r$. From Equations 1.5, 1.6 and 1.7

$$S(R) = \frac{-3kR^2}{2\beta M} + \text{terms that have no } R \text{ dependence.} \tag{1.8}$$

The free energy of a chain is $F = U - TS$, so now we need to know the potential energy $U(R)$. It turns out, however, that the potential is actually a slowly varying function of R for most end-to-end distances [12]. Since we will be looking for how the free energy changes with end-to-end distance, we cast U into the second set of terms in Equation 1.8 and say that the free energy is

$$F = \frac{3kTR^2}{2\beta M} + \text{other terms.} \tag{1.9}$$

As mentioned above, the free energy of a single polymer chain is quadratic in elongation. This is reminiscent of $U_{sp}(R) = \frac{1}{2}k_{sp}R^2$ however, as pointed out above and in the books [12, 13] the origin is quite different. Furthermore, the spring constant here is *proportional* to the temperature which means that a 'polymer spring' gets *stiffer* with increasing temperature. This is markedly different from a metallic spring because one of those springs actually gets *softer* as the temperature is increased.

ii Stretching a rubber

As stated earlier, a rubber is a system of polymer chains that are not allowed to slide past one another. Their entanglements are fixed in place but they are allowed to stretch in one

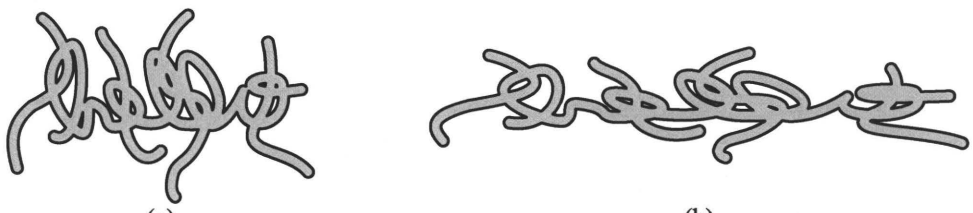

Figure 1.3: A 2D affine deformation: each part of the sample is deformed in proportion to the whole. The sample is stretched in the horizontal direction, but compressed in the vertical direction such that $W_o H_o = W_1 H_1$ where W and H refer to the width and height respectively.

direction or the other. Since they cannot slip and slide along, the system can be taken to be a collection of independent random walks, each with the same molecular weight as an entanglement strand, M_e. If the system is stretched, the factor by which the system has been stretched from its equilibrium length, λ, on average, also applies to each entanglement strand in the network [12, 13]. This is known as an *affine* deformation and a 2D example of it is shown in Figure 1.3.

Now assume that a rubber has been stretched in the x-direction and, to conserve volume, compressed in the y- and z-directions. If the initial displacements of a chain segment are x, y, z then the new displacements become[4] λx, $\frac{y}{\sqrt{\lambda}}$, $\frac{z}{\sqrt{\lambda}}$. If there are n entanglement strands in the system, then the change in free energy for the system from the initial state to the final state is just n times the change in free energy for a single strand. Given Equation 1.9, we get

$$\Delta F_{tot} = n\frac{3kT}{2\beta M_e}\left[(\lambda^2 - 1)x^2 + \left(\frac{1}{\lambda} - 1\right)(y^2 + z^2)\right].$$

From Equation 1.1, we know that the length component of a polymer chain is $x_i^2 = \beta M_e/3$ ($x_i \in \{x, y, z\}$). Because of this, we can write the change in free energy without reference to any specific chain, we just need to know the factor by which the system has been stretched:

$$\Delta F_{tot} = \frac{nkT}{2}\left[\lambda^2 + \frac{2}{\lambda} - 3\right]. \tag{1.10}$$

Now, to finish the argument as it is stated in [12] the force is the derivative of the free energy with respect to the length of the system, dF/dX. But $X = \lambda X_o$ so that $dX = X_o d\lambda$. This gives the x-component of force:

$$f_x = \frac{nkT}{X_o}\left[\lambda - \frac{1}{\lambda^2}\right]. \tag{1.11}$$

[4]More generally, the new coordinates are $\lambda_x x, \lambda_y y, \lambda_z z$, but since we require volume conservation it must be that $\lambda_x \lambda_y \lambda_z = 1$. Therefore if we extend in x by a factor λ and we require an isotropic deformation in y and z then $\lambda_y = \lambda_z = 1/\sqrt{\lambda}$.

The tensile stress is just the force per unit area $\sigma_{xx} = f_x/Y_oZ_o$ and the strain is $\gamma = \Delta X/X_o$ so that γ and λ are related by $\lambda = 1 + \gamma$. Finally, the volume of the system is $V = X_oY_oZ_o$ so that the stress-strain relationship is

$$\sigma_{xx} = \frac{nkT}{V}\left[(1+\gamma) - \frac{1}{(1+\gamma)^2}\right]. \tag{1.12}$$

The term before the square brackets in Equation 1.12 is known as the plateau shear modulus G_N^0, or for brevity, the plateau modulus. Since n is the number of entanglement strands in the system, n/V is just the density of cross-linked strands, ν_e. We have thus connected a material parameter to the molecular quantity which is the central theme of this thesis. If we remember that $\nu_e = \rho N_A/M_e$ we then have

$$G_N^0 = \frac{\rho N_A kT}{M_e}, \tag{1.13}$$

and to find a value of M_e we just need a method by which the plateau modulus G_N^0 can be measured at a known temperature and density. This topic will be discussed next. In order to understand how this quantity is measured, we will have to diverge into some theory about the viscoelasticity of polymers. Our math hands will get a little dirty, but we will be richer for it in the end.

iii The shear modulus (i): what is G?

Instead of considering a cross-linked rubber, we will now return our attention to a liquid system of polymers whose entangling interactions are not permanent. The present discussion will be concerned with a system subject to a definite, time dependent strain ($\gamma = \Delta X/X$ in the previous section) and the resulting stress (σ). This discussion has various parts of the work by Ferry [14] as well as references of the previous section [12, 13] as its inspiration; no attempt is made here to take credit for the ideas presented, though the words may be those of the author[5].

Since entanglements are not permanent interactions between a definite set of monomers, the imposition of some definite strain on a system will see the stress required to keep that strain decay as the polymer chains relax. The rate at which they relax depends upon the form of the shear modulus $G(t)$; a typical form for the function is shown in Figure 1.4. For early times, $G(t)$ is peaked and it is during this time regime when the system acts like a glassy solid. The molecules making up the system have not yet realized that they are springy objects, it is not until the intermediate time regime, $\tau_g \leq t \leq \tau_r$, that the chains feel this effect. During intermediate times $G(t)$ is constant and has the value of the plateau modulus,

[5]The same could be said of the references from the previous section

G_N^0. This is because the entanglements that make up the polymer network have not had time to relax, and for this period of time they act like the cross-links described in the previous section. After some terminal time, τ_r, the chains relax and reptate out of the confinements which initially held them. At this point, less and less stress is required to hold the system at a given strain since the chains have had time to wriggle from their constraining enanglements and their end-to-end distances are becoming shorter (see Equation 1.9). Considering the chains shown in Figure 1.1, one can imagine that the network is strained such that the lateral chain becomes elongated as in Figure 1.5(a). After τ_r though, thermal fluctuations have allowed the chain to find its entropy-preferred random walk trajectory, as in Figure 1.5(b), at the expense of the original entanglement configuration.

The relationship between stress and strain for a polymeric system can be written

$$\sigma(t) = \int_{-\infty}^{t} G(t-\tau)\dot{\gamma}(\tau)\, d\tau. \tag{1.14}$$

The integral is over all past times, and given the schematic of Figure 1.4 it can be seen that the most recent strain events make the largest contribution to the stress. The form as given by Equation 1.14 indicates that all past strain events influence how the polymers will deform, or that the system has *memory*. It is noted that each event is weighted linearly in the strain rate $\dot{\gamma}$, but is progressively damped by the function G as time elapses. Other expressions can be written if the stress is a more complicated function of the strain, for example if it follows a different power law, $d\sigma(t) = G_m(t-\tau)\dot{\gamma}^m\, d\tau$, or if it is some other more complicated superposition of past and present strains: $\sigma(t) = \Psi\left[\gamma(t), \dot{\gamma}(t), G_\Psi(t)\right]$. In this work, we will confine ourselves to the linear rule of Equation 1.14, since for a given system the strain response can always be modeled linearly if the strains are small enough.

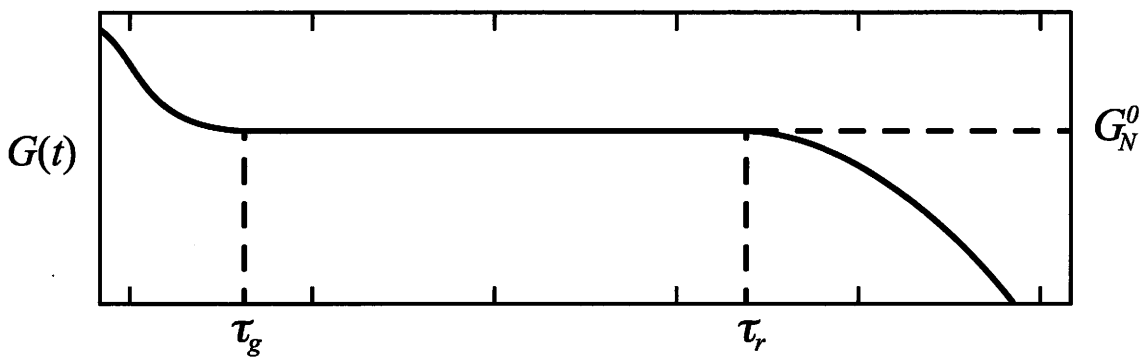

Figure 1.4: The shear modulus of a typical polymer system as a function of time. Note that both axes are logarithmic, so that the glass like regime (early times) is actually many orders of magnitude shorter lived than either of the proceeding (plateau or terminal) time regimes.

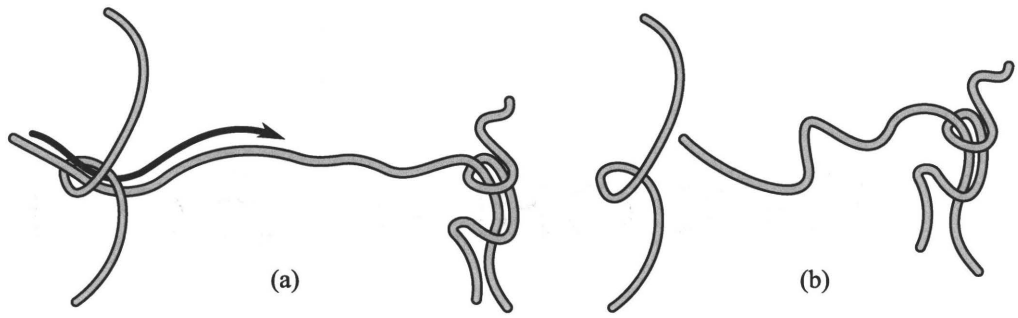

Figure 1.5: Immediately after network deformation, the chains are stretched out as in (a), but (b) thermal fluctuations allow the chains to find their equilibrium Gaussian configurations anew.

To make the significance of $G(t)$ somewhat more clear, consider the strain profile shown in Figure 1.6. The system is represented by the grey box on the left of Figure 1.6 and at $t = -\xi$ is subjected to a small constant shear rate (dashed line) which continues until $t = 0$. After this time, the box has been sheared by some amount γ_o, and has the shape as shown on the right of Figure 1.6. For all times outside the interval $-\xi \leq t \leq 0$ the shear rate is $\dot{\gamma} = 0$. For this experiment, the stress on the system for all subsequent time is given by Equation 1.14 as

$$\sigma(t) = \frac{\gamma_o}{\xi} \int_{-\xi}^{0} G(t - \tau)\, d\tau.$$

In calculus, the mean value theorem tells us that any definite integral $I = \int_a^b f(x)\, dx$, over a smooth function can be by found taking the interval of integration $(b - a)$, and multiplying that by a value of the function somewhere in that interval $f(\tilde{x})$ where $a \leq \tilde{x} \leq b$: $I = (b - a) \times f(\tilde{x})$. This theorem can be used to simplify the preceding expression for $\sigma(t)$

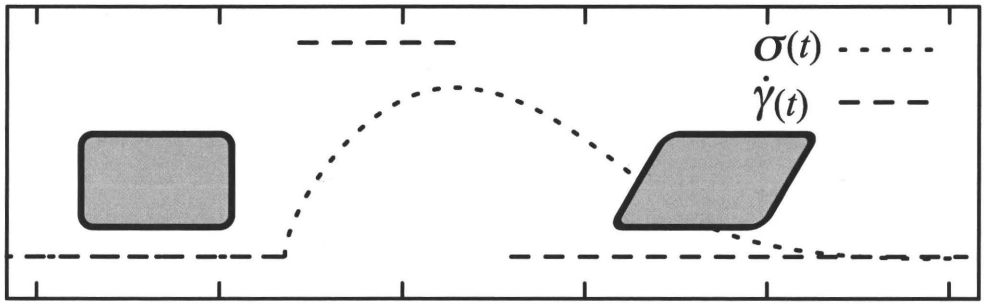

Figure 1.6: A simple experiment in which a polymer system (grey box) is sheared by some amount γ then held fixed. $\dot{\gamma}$ and σ are respectively, the rate-of-strain and stress and their time dependence is shown as the dashed and dotted lines. The vertical scales are arbitrary.

because $\int_{-\xi}^{0} G(t-\tau)\ d\tau = \xi G(t+\epsilon\xi)$ and we can write

$$\sigma(t) = \frac{\gamma_o}{\xi}\xi G(t-\epsilon\xi).$$

This expression can be further simplified by remembering that ξ is actually a short time span, that $0 \leq \epsilon \leq 1$, and by considering times $t \gg \xi$ so that

$$\sigma(t) = \gamma_o G(t). \tag{1.15}$$

From this expression, the physical meaning of $G(t)$ can now be clearly seen. If a system is strained by some amount γ_o, then $G(t)$ regulates the amount of stress $\sigma(t)$ required to hold that deformation for all subsequent times. Actually, Equation 1.14 can just be seen as the sum of many infinitesimal step strains $d\gamma$, over short time periods $d\tau$.

iv The shear modulus (ii): oscillatory experiments

Much of the literature that reports values of M_e have come by the numbers after performing oscillatory shear experiments [6, 7] (and most of the references therein). This fact motivates all of the previous discussion about the entropy of a chain, the shear modulus *et cetera*. Imagine a liquid polymer sample in which the chains all have $M \gg M_e$ confined between two plates. In oscillatory shear experiments, one of the plates is driven to harmonically oscillate at some specified frequency ω and the resulting stress on the opposite plate is measured once the steady state is reached.

If the strain as a function of time is given by $\gamma(t) = \gamma_o \sin(\omega t)$ then the stress as a function of time can be found by substitution of $\dot{\gamma}$ into Equation 1.14

$$\sigma(t) = \int_{-\infty}^{t} G(t-\tau)\ \gamma_o \omega \cos(\omega\tau)\ d\tau,$$

where the $\dot{\gamma}(\tau) \sim \omega\cos(\omega\tau)$ and γ_o is again a small and constant strain. An enlightening change of variables can be made at this point. Having $s = t - \tau$ gives

$$\begin{aligned}\sigma(t) &= \gamma_o\omega \int_0^{\infty} G(s)\ \cos(\omega(t-s))\ ds, \\ &= \gamma_o\omega \int_0^{\infty} G(s)\ [\sin(\omega s)\sin(\omega t) + \cos(\omega s)\cos(\omega t)]\ ds,\end{aligned}$$

and the important result is

$$\sigma(t) = \gamma_o \left[\omega \int_0^{\infty} G(s)\sin(\omega s)\ ds\right] \sin(\omega t) + \gamma_o \left[\omega \int_0^{\infty} G(s)\cos(\omega s)\ ds\right] \cos(\omega t); \tag{1.16}$$

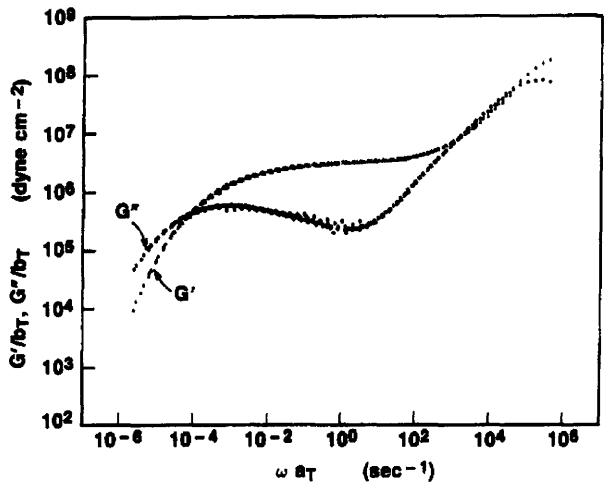

Figure 1.7: The storage G', and loss G'', moduli for a polyisobutylene sample as seen in [15]. G'' is the curve that has the minimum at $\omega a_T \simeq 10^0$ s^{-1} while G' is the curve which has a relatively flat region at the same frequency. a_T and b_T are temperature dependent shift parameters. Often a given apparatus is only capable of operating in a limited frequency window. In order to probe a larger effective range, it is possible to do experiments at different temperatures and then to use reduced variables. In this way, an experiment done with (ω_1, T_1) can be compared to an experiment done with (ω_1, T_2) as if it was done at the same temperature as the first experiment, but at a different frequency, (ω_2, T_1).

this can be said in a more pedagogical way, and that is to say

$$\sigma(t) = \gamma_o \times \Big[\text{a function of } \omega\Big] \times \sin(\omega t) + \gamma_o \times \Big[\text{another function of } \omega\Big] \times \cos(\omega t).$$

So we see that the stress oscillates with a magnitude A, at the same frequency as the imposed strain but that it is out of phase with the driving by some amount δ. A and δ both depend on the values of the 'functions of ω' from Equation 1.16. The part that modulates the 'sin' term is known as the storage modulus, $G'(\omega)$, and the part that modulates the 'cos' term is known as the loss modulus, $G''(\omega)$. To be explicit, the storage and loss moduli are

$$\begin{aligned} G'(\omega) &= \omega \int_0^\infty G(s) \sin(\omega s)\, ds, \\ G''(\omega) &= \omega \int_0^\infty G(s) \cos(\omega s)\, ds, \end{aligned} \tag{1.17}$$

and typical forms for them are shown in Figure 1.7 as seen in [15]. As we will see, these functions will be central to the determination of G_N^0.

The origin of the terms 'storage' and 'loss' modulus can be understood in reference to the stress felt by purely elastic or purely viscous systems. In the elastic case, the stress is given by Hooke's law, $\sigma = G_N^0 \gamma$ and if $\gamma(t) \sim \sin(\omega t)$ then it follows that the stress is

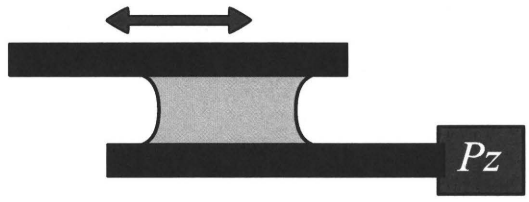

Figure 1.8: A polymer system is sheared at frequency ω by the top plate and the resulting stress is measured by Pz, the piezoelectric crystal which is mounted on the bottom plate.

also proportional to $\sin(\omega t)$. In a purely Hookean system all of the energy is in the form of kinetic energy, or else it is *stored* in the 'springs' that make up the system. If the system is a Newtonian liquid though, the stress on the system is given by $\sigma = \eta\dot{\gamma}$ and for the same imposed strain as above the stress is instead proportional to $\cos(\omega t)$. For these systems, all of the input energy is eventually converted to heat by viscous dissipation; it is essentially *lost*. To sum up, the loss modulus describes the viscous behaviour of the system and the storage modulus describes the elastic behaviour.

In almost all of the literature cited at the beginning of this section, little reference is ever made to the storage modulus. Instead, measurement of $G''(\omega)$ over a wide range of ω is used to determine G_N^0 and ultimately M_e or ν_e; the method by which this is done can now finally be discussed. One way to get the loss modulus as a function of ω, is to shear a polymer melt confined between two plates with $\gamma = \gamma_o \cos(\omega t)$ by oscillating one of the plates. Measurement of the resulting stress as $\sigma(t) = A\cos(\omega t + \delta)$ is done by mounting a piezoelectric ceramic onto the other, 'fixed' plate. This type of experiment is shown schematically in Figure 1.8. The values of A and δ obtained can be used to calculate both the storage and loss moduli $G'(\omega)$ and $G''(\omega)$ for the frequency used in the experiment. Thus, G'' can be measured at any frequency (and temperature) convenient for the apparatus.

To get G_N^0 from the G'' spectrum, we need some way of inverting Equation 1.17 since oscillatory experiments actually *measure* $G''(\omega)$ and not $G(t)$. One way of transforming a function of ω into a function of t is to multiply the original function $(G''(\omega))$ by some function of ω and t and integrating with respect to ω. Dividing 1.17 by ω, multiplying by a fortuitous choice of function and integrating gives

$$\int \frac{G''(\omega)}{\omega} \cos(\omega t)\, d\omega = \iint G(s)\cos(\omega s)\, ds \cos(\omega t)\, d\omega,$$

changing the order of integration on the right hand side reveals a delta function

$$\int \frac{G''(\omega)}{\omega} \cos(\omega t)\, d\omega = \int G(s)\, ds \int \cos(\omega s)\cos(\omega t)\, d\omega,$$
$$= \int G(s)\, \frac{\pi}{2}\delta(s-t)\, ds,$$

$$\frac{2}{\pi}\int_0^\infty \frac{G''(\omega)}{\omega} \cos(\omega t)\, d\omega = G(t). \tag{1.18}$$

So by integrating the experimentally determined loss modulus, one can obtain the shear modulus function, $G(t)$ for any desired value of t.

To get G_N^0 requires one to know a value of t that is between τ_g and τ_r in Figure 1.4, lets call the value of t which is half way between them t_N^0. Then it is true that

$$G_N^0 = G(t_N^0) = \frac{2}{\pi}\int_0^\infty \frac{G''(\omega)}{\omega} \cos(\omega t_N^0)\, d\omega,$$

this, though, requires G'' for large ω and worse, requires *a priori* knowledge of t_N^0.

Referring to Figure 1.7 one sees that there is a minimum in $G''(\omega)$ at $\omega a_T \simeq 1$ Hz with a correspondingly large value of the storage modulus at the same frequency; lets say that the frequency for which G'' is minimized is called ω_{min}. The frequency at which there is a minimum in the ratio, G''/G' is the frequency for which there is a minimum in the proportion of energy which is lost due to viscous effects. If there is minimal viscous energy dissipation at ω_{min}, then at that frequency there must be a correspondingly large proportion of energy stored in the system. At this frequency the system acts most like a Hookean solid.

If one substitutes $t = 0$ in Equation 1.18, integration of $G''(\omega)$ gives $G(0)$, or the value of the shear modulus describing glassy behaviour (see Figure 1.4). The popular procedure

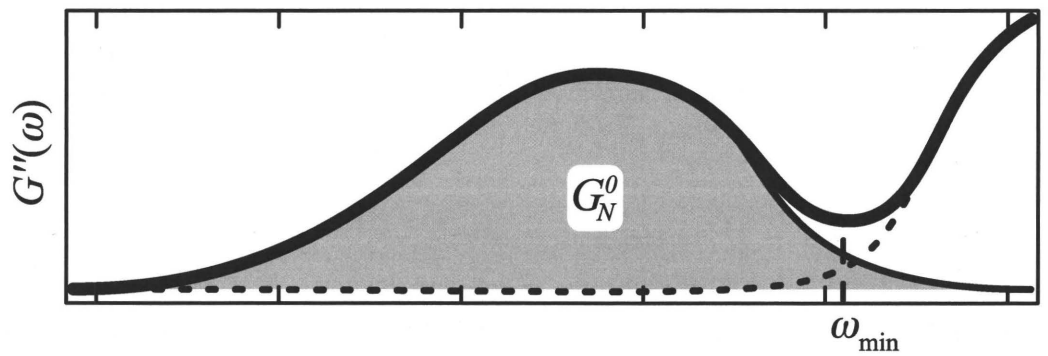

Figure 1.9: Decomposition of the loss modulus (thick solid line) into two peaks. The glassy peak (dotted line) and the viscoelastic peak (G''_{lfp}, thin solid line) whose integration gives the plateau modulus, G_N^0.

for finding G_N^0 is to say that ω_{min} is approximately the point of overlap between two peaks that make up $G''(\omega)$. The high frequency peak, corresponding to times $t < \tau_g$, is the peak describing the glassy behaviour of the system. The low frequency peak, corresponding to times $t > \tau_g$, is the one that describes the viscoelastic behaviour of the system. The decomposition of G'' into two peaks is shown schematically in Figure 1.9. So, if one only considers the contribution due to the low frequency peak and substitutes $t = 0$ in Equation 1.18, the resulting integral is taken as the plateau modulus

$$G_N^0 = \int_0^\infty \frac{G''_{lfp}(\omega)}{\omega}\, d\omega, \tag{1.19}$$

where $G''_{lfp}(\omega)$ is the portion of the loss modulus which is taken to be the low frequency peak. One of the earliest occurrences of this method is found in [16]. This is the work cited by Ferry [14], and Ferry is in turn the work cited by a large number of authors when G_N^0 is determined from the loss modulus [6, 15, 17, 18, 19, 20]. This method has been compared [20] to at least two other methods for determining G_N^0 from viscoelastic data and the methods appear to be consistent. As well, Roovers [18] has compared the theory developed by Doi and Edwards [21, 22] which does not take into account the mechanisms that give rise to the second peak seen in Figures 1.7 and 1.9. In that work Roovers showed that the agreement between theory and G''_{lfp} was good.

If one has acquired the frequency dependence of G'' through the use of oscillatory shear experiments, it is then possible to use G''_{lfp} to get the plateau modulus. Since from Equation 1.13 the plateau modulus is inversely proportional to the entanglement molecular weight,

$$G_N^0 = \frac{\rho N_A kT}{M_e},$$

this provides us with a value for M_e.

IV Crazing

Crazing is an energy dissipation mechanism in *glassy* polymer systems. If enough tension is applied to a polymer glass a large amount of strain, compared to other glassy systems, may be imparted to it. The way that polymer glasses distribute strain through a system, however, is rather different than the affine deformations that take place in ductile metals or rubbery systems such as is shown in Figure 1.3, and the way they deform is also different from other glassy systems in which the molecules are not long polymers.

When a glassy system of small molecules is stressed past the yield point, a crack may form and the glass fractures shortly thereafter; windows shatter by this mechanism. For polymers with molecular weights $M < M_e$ this type of brittle failure may take place. However, when

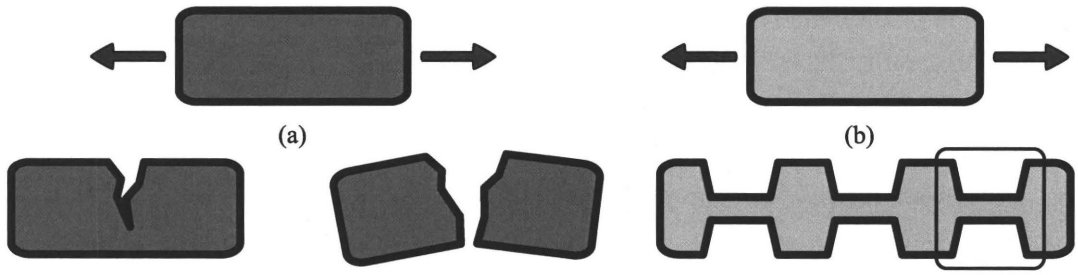

Figure 1.10: Side view of two deformation modes. A glass of small molecules (a) often shatters soon after the onset of large scale system deformation; however (b) when the glass is made up of molecules with large molecular weights $M \gg M_e$, the system will exhibit crazes, three of which are shown here. A top view of a single craze (boxed region in (b)) is shown in Figure 1.11

the chains mostly have $M \gg M_e$ they deform by a quite different mechanism and much more energy is required to break the system apart [23]. Rather than immediately shattering like a window pane, there is an intermediate step which can be seen as a ductile regime, and that is the regime of crazing. Crazes are deformed polymer that appear throughout the system. A portion of the sample is elongated in the same direction as the applied stress, but compressed perpendicularly, and the surrounding material is left undeformed. Since the deformation occurs only in specific regions in the sample it is non-affine. The contrast between these two deformation modes is shown schematically in Figure 1.10 as a side view.

The corresponding top view is shown in Figures 1.11 and are optical microscopy and atomic force microscopy (AFM) images of crazed PS. The picture shown in Figure 1.10 is somewhat of a simplification since craze fibrils are not indicated there. However, even on the scale of the optical microscopy image shown in Figure 1.11(a) the craze fibrils cannot be resolved. The crazes were grown in samples which were approximately 130 nm thick and

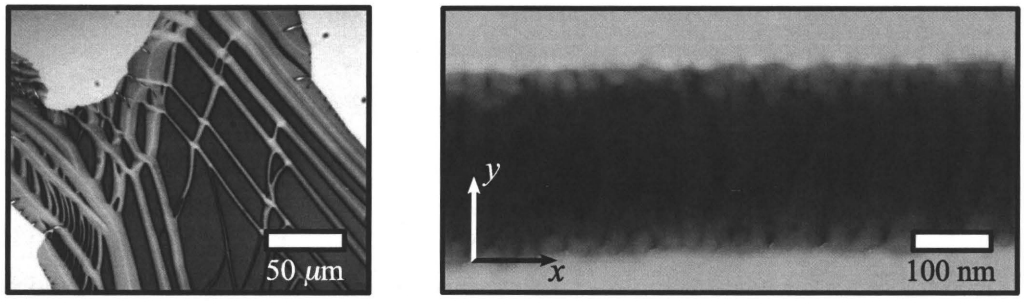

Figure 1.11: (a) optical microscopy and atomic force microscopy images of crazes grown in PS samples. The scale bars are approximate.

about 5×5 mm^2. The image in (a) is an optical microscopy image and the brightest areas are a reflective substrate, the darkest areas are uncrazed polymer and the rest is crazed material. In (b), the image is an atomic force microscopy topography relief (darkest areas are small heights and the brightest areas are higher). Near the top and bottom of the figure, there is undeformed polymer material which is bridged by the craze fibrils shown in the centre. In (b) the stress was applied vertically as opposed to the schematic in Figure 1.10 where it is shown being stressed horizontally and opposed to (a) in which strain was applied in many directions.

The craze regions are clearly anisotropic; the fibrils are preferentially oriented in the direction of applied stress. This need not always be the case though, for a different polymer, or even with the same polymer in a different environment, it is possible that the 'craze' regions will not contain any voids as shown in Figure 1.11(b). In these cases, the deformed regions are not called 'crazes' but are called 'deformation zones.' Since all the samples studied here deformed by crazing, we will pay no further attention to the alternative method.

i Craze growth

Crazes are formed from an isotropic solid which means that they must nucleate and grow before they take the form seen in Figures 1.10(b) and 1.11. Several authors have studied various aspects of craze nucleation [1, 3, 24] but this process is not directly related to the results presented in this thesis and therefore will not be discussed. A similar statement can be made concerning the failure of crazes [2, 3, 25, 26]. We will concern ourselves here with the process of craze growth. Later we will see how comparison of the polymer which has been crazed to the polymer which is uncrazed can explain how a polymer chain's length affects its ability to participate in global system events.

If the stress applied to a polymer sample is uniaxial, crazes form in parallel. A wider view of Figure 1.11 would almost see that figure as the 'unit cell,' except that there would be more uncrazed material between the crazes, and the crazes are not infinitely long in the horizontal direction. Actually, this calls to question the title of this section. Let us assume that a craze has already been formed, then we want to know how the existing crazes grow. There are three methods by which this can happen: (1) the craze tip (not shown in Figure 1.11; the walls between crazed and uncrazed material eventually converge far to the left and right of the bounds in this figure) may advance to make the craze in Figure 1.11 wider in the x direction; (2) the walls of the craze may advance upward (or downward), bringing new material into the craze and making it wider in the y direction; and (3) the existing material in the craze can become more deformed (the fibrils of Figure 1.11 would become taller and thinner) also making the craze wider in the y direction.

The crazes we study in this work are grown in films roughly 130 nm thick. Given the

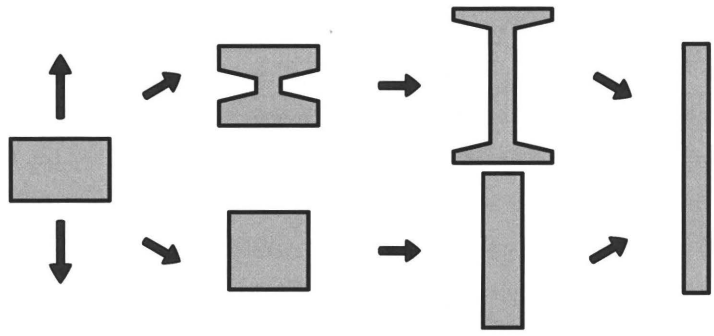

Figure 1.12: Craze thickening mechanisms. In both cases, the initial and final products are the same, but the intermediate steps are different. In the upper pathway (surface drawing) the craze thickens by drawing new material into the craze while in the bottom pathway (fibril creep), the craze thickens by further deforming the existing crazed material.

coordinate system defined in Figure 1.11, they are typically of order 10 μm wide in the y-direction [6] , and can extend a millimetre or two in the x-direction; craze tip advance (1) is the process that allows crazes to have such a large extent in this direction. Close to the craze tip, the thickness in the y-direction is only about 4 nm [25], which is much less than the typical 10 μm quoted above. Since this is the case, there must be significant contributions to craze growth from either of craze thickening methods (2) and (3) from above. The two methods by which a craze can thicken in the y-direction are shown schematically in Figure 1.12.

At the extreme left, the figure shows a piece of material that goes into making a craze. At the extreme right, the final state of the material is shown [7]. In the top thickening pathway, the craze grows by drawing new, uncrazed material into the existing deformed material. This adds to the volume of crazed material and takes away from that of the uncrazed volume. In the bottom, it grows by continually deforming the already crazed material. These two craze thickening mechanisms are known as the surface drawing and fibril creep, respectively [25].

If fibril creep is the dominant mechanism of craze thickening, then the system must somehow decide *a priori* how much material will be crazed. Fibril creep would also give rise to a correlation between the craze thickness and the degree of deformation of polymers in the craze. On the other hand, if surface drawing is the dominant mechanism, the amount of crazed material will depend only on the extent to which the system has been deformed as a whole. While it is not necessary that only one of these craze thickening mechanisms operate in the crazing process, it is possible that one will dominate the deformation. In the

[6] The craze fibrils in Figure 1.11 would not be well resolved in an AFM scan 10μm wide. So, this figure is not quite 'typical' of a mature craze, but it serves the purpose of illustrating crazed and uncrazed material in one place.

[7] Note that crazing is a plastic deformation process, so it is assumed that the volume of material remains constant before and after crazing [25].

experimental studies of crazing by Lauterwasser and Kramer [25] and by Brown [27], and in the simulations by Rottler and Robbins [2], it has been shown that surface drawing is indeed the dominant craze thickening mechanism. In [25] and [27], it was shown that there is no correlation between the extent of deformation in a craze and the craze thickness [8] .

ii The connection between craze and chain dimensions

Earlier it was said that our aim was to understand what happens to a polymer network when the entanglements that hold it together are swelled. To do this, we have studied the results of crazing experiments. Because our experiments do not directly measure individual chains, it is necessary to connect the results of the experiments to the molecular quantities of interest.

When a glassy polymer system is strained and crazes are formed, it seems clear from Figure 1.11 that even the craze regions are not affine deformations. In their simulations of craze growth and fracture though, Rottler and Robbins [2] were able to show that crazes can be taken to be deformations that are *statistically* affine. This of course applies only to the regions of the sample that were actually deformed, and not to the system as a whole (see Figure 1.10). The type of deformation depicted in the boxed portion of Figure 1.10 can therefore be considered as affine.

Now, we need to consider that the individual polymer molecules making up the system must also become deformed. The question of what they look like before and after the deformation will now be discussed. First though, a comment concerning entanglements in a polymer glass is in order. In the melt one must distinguish carefully between entanglements and cross-links since the structure of individual molecules greatly influences their mobility [28]. Since entanglements are not permanent connections, an applied stress to a melt may cause two entangled molecules to disentangle and become spatially separated as shown in Figure 1.5. It is much less likely for an applied stress to break chemical bonds (as long as it is not too large) hence cross-linked chains remain in contact under the same applied stress. Cross-linked chains are harder to push around one another than similarly sized linear chains.

In the glassy state, the difference between entanglements and cross-links, however, is not so clear. In a polymer melt, each chain wriggles and reptates about and interacts with many different chains over time. As T_g is approached, though, the chain interacts with fewer chains over the same period of time. When the temperature is below T_g, the quasiequilibrium interactions between one chain and its neighbours becomes fixed in time. Since this is the

[8] Actually, this is not the whole story. Near the craze tip, the extent of deformation in the craze is somewhat higher than that for material far away from the craze tip. This has been explained [25] by arguing that the amount of stress required to *widen* a craze by propagating the tip is actually greater than the amount of stress required to *thicken* it. Thus, one sees is a small region in the middle of a craze, called a 'midrib', where the polymers have been deformed to a slightly larger extent compared to the rest of the craze.

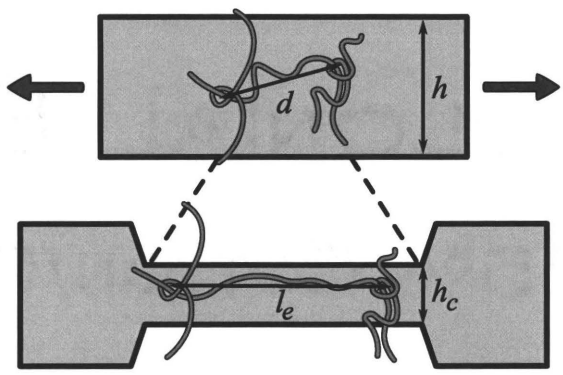

Figure 1.13: At the top, an undeformed polymer glass, of height h has chains with random walk trajectories, and the distance between entanglements is d. In the crazed section of the glass, whose height is h_c, the new distance between entanglements is l_e. One should consider the scale of the 'system' which is being strained here to be of order 100 nm tall and of order 1 mm wide. The polymer chains depicted here, though, should be considered as having sizes of about 10s of nanometres.

case, one might infer that the entangling interactions which slow the rearrangements of polymer chains in the melt might become something of a 'cross-link' in a glass. For the purposes of crazing experiments it has indeed been shown by Donald and Kramer [11] that one may treat entanglements in polymer glasses as permanent connections between the chains. If experiments are done near T_g, though, disentanglement [29] may occur due to reptation of the polymer on the time scale of an experiment. In these cases entanglements may not be treated as permanent interactions between a definite set of monomers, and care must be taken with how to interpret results in these types of experiments.

In a polymer glass that has been frozen from an equilibrated melt, the chain configurations are random walks as depicted in Figure 1.1. After the deformation that takes place in Figure 1.10(b) though, the polymer chains that are part of the craze regions are no longer random walks at all. They have been given some preferred orientation as a result of the straining. A schematic of the state of polymer chains in strained and unstrained glasses is shown in Figure 1.13.

In the model presented by Donald and Kramer [11], the following assumptions are made. In an uncrazed polymer glass, the trajectories of a polymer chain are random walks[9]. Therefore, given Equation 1.1, we have $d \sim M_e^{\frac{1}{2}}$. After the crazing process has completed, the trajectories are no longer random walks so the distance between entanglements should then scale linearly in the amount of material between entanglements, that is, $l_e \sim M_e$. In both of these statements it is assumed that the length of chain segments between entanglements remains constant. This implies the above discussion concerning entanglements *vs.* cross-links

[9]For an alternative model that does not consider the polymer chains as random walks, see Appendix A.

in polymer glasses. Comparing the distances between entanglements before and after the crazing process, we have

$$\lambda \equiv \frac{d}{l_e} \sim M_e^{-\frac{1}{2}}, \tag{1.20}$$

where λ is called the extension ratio of the molecules. So if one can measure or infer l_e and d, this relationship gives a measure of M_e, or at the least, a method by which M_e can be compared from one system to the next.

In the next chapter, it will be discussed that the experimentally measured quantities that make up the most important parts of this work are the heights h_c and h. These heights are shown in the 'system' of Figure 1.13, h is the height of the uncrazed material and h_c is the height of the craze. The purpose of this section is to connect these quantities to the ones that make up Equation 1.20. To do this we first assume that, as pointed out in [2], there is no *net* change in the out-of-plane dimension of the system during crazing. Let the width of the craze be called w_c and let the width of material that went into making the craze be w_o. Then if volume is conserved during crazing, it must be true that

$$hw_o = h_c w_c, \tag{1.21}$$

where the out-of-plane dimension cancels because it is unchanged. Finally, we assert that the deformation of the system is a manifestation of the collective deformations of all of the polymers that make it up. If this is true, then we can write

$$\frac{w_o}{w_c} = \frac{d}{l_e},$$

and given Equations 1.20 and 1.21, we can now compare the entanglement molecular weights of different systems by crazing them and measuring both the deformed and undeformed heights:

$$\frac{h_c}{h} \sim M_e^{-\frac{1}{2}}, \tag{1.22}$$

and given Equations 1.20 and 1.22, we see that

$$\left(\frac{h_c}{h}\right)^2 \sim \nu_e. \tag{1.23}$$

It may not be an overstatement to say that this relationship is the one that gives meaning to almost all of the results that are to be presented later in this thesis.

iii Measuring λ

Several methods have appeared for measuring the extension ratio, λ, in crazed polymer glasses and a decent summary of them is listed in [30]. The first method by Kambour [31]

was an optical technique that used total internal reflection in crazes to measure their density. This density was compared to the bulk density of crazed matter and from this, the volume fraction, v_f, could be computed as the ratio of the craze density to the bulk density. After v_f is computed, it is easy to show that $\lambda = 1/v_f$.

Here, the craze density is the average density of material in the craze region. The volume used in computing this density can be defined by the craze width, w_c and the *original* height of the sample, h. The 'craze density' does not reflect a change in the density of polystyrene in the craze, it merely reflects the fact that there are voids interspersed between craze fibrils and the craze density must therefore be less than the bulk density.

Methods for measuring v_f by using the scattering vectors of x-rays have also been devised [30]. The method by which one can determine λ by AFM was discussed above and has appeared at least twice [4, 32]. AFM was also responsible [33] for the 'discovery' that craze fibrils gather into clusters (at least in thin films) near the middle of the craze region as seen in Figure 1.11 and in the schematics of crazing discussed in this section. Previous to these observations of 'craze necks,' (as late as 1990, see Figure 3 of [34]) it was supposed that craze fibrils were distributed uniformly through craze regions.

The most widely used method, however, has been that developed almost simultaneously by Kramer [25] and Brown [27]. In this method transmission electron microscopy (TEM) is used to image, simultaneously, a hole, some crazed material and undeformed regions in a polymer glass. The basic idea is that electrons incident on a sample of a given thickness may or may not be scattered by some angle. The probability that a sample scatters an electron by some angle θ_{max} or greater is a function of the thickness of the sample.

For samples that are not too thick, it can be shown [25, 35] the probability of scattering at an angle greater than θ_{max}, which is the angle subtended by an aperture below the sample in a TEM, is an exponentially decreasing function of the thickness of the sample. Hence,

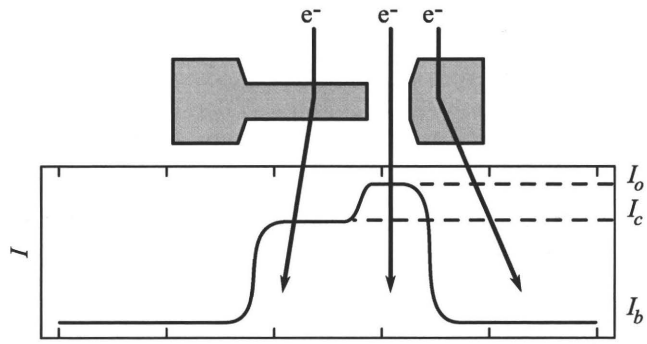

Figure 1.14: Electrons incident on a sample of varying thickness have some probability of being scattered out of the viewing area. The thicker the specimen, the more likely is it for an electron to be scattered out. This gives rise to a position dependent intensity profile.

the intensities of crazed and uncrazed material in the film as measured on a CCD camera ought to have the form

$$\begin{aligned} I_c &= I_o e^{-\frac{h_c}{\ell}}, \\ I_b &= I_o e^{-\frac{h}{\ell}}, \end{aligned} \tag{1.24}$$

where I_o and ℓ are both constants for a given experiment. I_o is simply the value of the intensity as measured in a hole and ℓ is a measure of the mean free path for the electron. If Equation 1.24 is true, then one can calculate the ratio of h_c and h from the measured intensities via

$$\frac{h_c}{h} = 1 - \frac{\ln(I_c/I_b)}{\ln(I_o/I_b)}. \tag{1.25}$$

With the use of Equation 1.23, one can determine λ for the crazed material by extracting values of I_o, I_c and I_b after having measured an intensity profile like the one shown in Figure 1.14.

V Swelling entanglements

The question of what happens to a polymer system when the entanglements that hold it together are swelled is addressed in this work. The method by which we affect this swelling, and certain effects one should expect to see, will presently be discussed. Figure 1.15 schematically shows how one might swell entanglements, and that is to move all entanglements apart along the chains. Practically, though, this would be hard to do in an equilibrated system.

Rather than trying to actually separate entanglements in the system, our approach has been to render some of the entanglements in a system incapable of transferring stress across the network. Consider a network that is composed of chains with molecular weight that is much greater than M_e as shown in Figure 1.16(a). In this case, the length scale describing entanglements is d_1. Now a similar system is prepared in which some of the long chains are

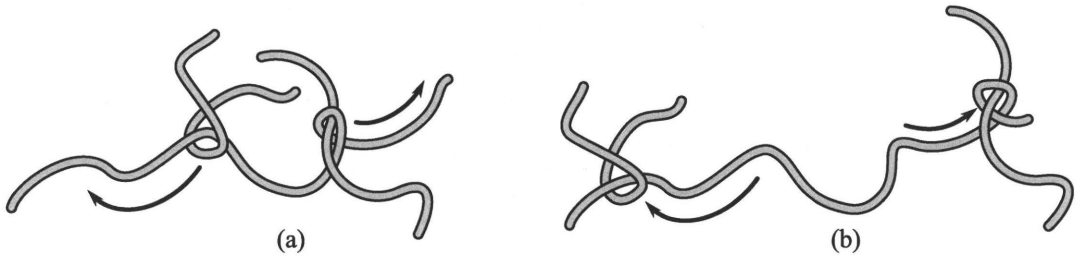

Figure 1.15: Initially the entanglements are (a) close together and M_e is small, but then they are farther apart after (b) the network has been swelled and M_e is large.

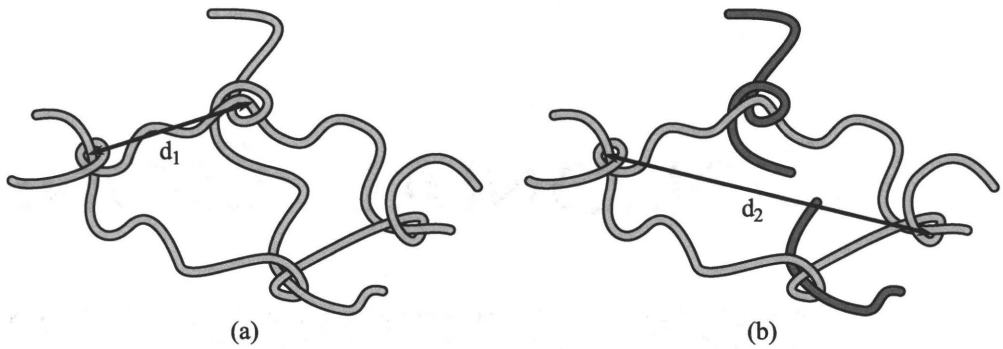

Figure 1.16: Before 'cutting' long chains (a) the relevant length scale in the system is d_1. After cutting some of the polymer chains, the new relevant length scale is d_2.

cut into many pieces. Assume that each new piece has a molecular weight which is smaller or comparable to M_e, as shown in Figure 1.16(b). In this case, the entanglements that resulted from interactions with the vertical chain have been made incapable of holding tension between the two horizontal ones. Since this is the case, the new length scale describing entanglements is d_2.

Practically, it is not possible to controllably 'cut' polymer chains into monodisperse lengths. However, it is possible to create relatively monodisperse collections over a wide range of molecular weights both above and below M_e for many polymers and, in particluar, PS is one of them. In the following, the symbol M_- will be used to denote chains whose molecular weights are smaller or comparable to M_e: $M_- \lesssim M_e$. As well, M_+ will be used to refer to chains whose molecular weight is much greater that M_e: $M_+ \gg M_e$.

To reduce the number of entanglements in a system continuously, the idea is to prepare systems that are blends of M_- and M_+ chains. More precisely, some weight fraction, ϕ, of the chains have molecular weights M_-. The rest of the system, $(1-\phi)$, is composed of polymer chains with molecular weights M_+. In these system, there are three broad categories of interactions between chains and they are summarized in Figure 1.17. Interactions between two M_+ chains are denoted $++$, interactions between a big chain and a short chain are denoted $+-$ or equivalently by $-+$, and interactions between two M_- chains are denoted $--$.

The entanglement density, ν_e, is a material parameter that is not much affected by the molecular weight of the chains that make up the system. However, one can imagine that by reducing the molecular weight of the chains in the system, some measurable change must take place. Here we define an *effective* entanglement density, ν_{eff}, and a corresponding effective entanglement molecular weight, $M_{eff} \sim 1/\nu_{eff}$, that describe the change that takes place as a result of a change in, specifically here, ϕ for the system. When ϕ is small, the interactions are dominated by $++$ interactions, because these are interactions between chains that have

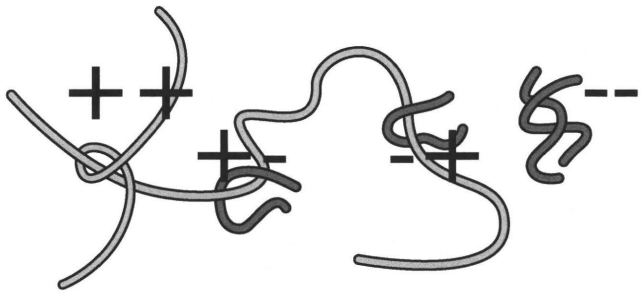

Figure 1.17: There are entanglements between big chains (++), between big chains and short chains (+− or −+), and there are entanglements between short chains (−−).

large molecular weights. Conversely, when ϕ is large, the majority of interactions are $--$ because in this situation the system is composed mostly of short chains.

If it can be assumed that entanglements are the result of interactions between groups of monomers on individual chains, then it becomes relatively easy to write down how ν_{eff} should change with ϕ. The analysis amounts to asking, "if I pick two groups of monomers from two specific chains, what is the probability that they come from a long or a short chain?" In a system with a given ϕ, the probability that the monomers both come from chains with M_- is $P(--) = \phi^2$. Similarly the probability for choosing monomers from two long chains is $P(++) = (1-\phi)^2$. The probability for choosing monomers from a long and a short chain is $P(+-) = 2\phi(1-\phi)$ and it is true that $P(++) + P(+-) + P(--) = 1$.

In the systems that are discussed in this thesis, there are chains with molecular weights M_+ and M_-. Since $M_+ \gg M_e$ it is expected that all the interactions between big chains will lead to entanglements. However, since the short chains have $M_- \lesssim M_e$ we expect that only some of the $+-$ and $--$ interactions will lead to entanglements. Given these assumptions we can write down how the *effective* entanglement density should scale with ϕ:

$$\nu_{eff} = \nu_e \left[(1-\phi)^2 + 2a\phi(1-\phi) + b\phi^2\right], \tag{1.26}$$

where a and b are the parameters that describe the probability that interactions between a short chain and another chain in the system contributes to the effective entanglement density. ν_e is the entanglement density of the polymer species. In order to connect this to the measured values (h_c and h) in our experiments, we just need to remember that the ratio of these two measurements is a function of M_e as shown in Equation 1.22. As well, since $M_e \sim 1/\nu_e$, $(h_c/h)^2$ will have the same dependence on ϕ as in Equation 1.26, except instead of having the prefactor ν_e, we will have

$$\left(\frac{h_c}{h}\right)^2 = \lambda_o^{-2}\left[(1-\phi)^2 + 2a\phi(1-\phi) + b\phi^2\right], \tag{1.27}$$

where λ_o^{-2} is a constant for a given polymer species and a and b are the same as in Equation 1.26.

This method of reducing the network's ability to transfer stress through the system has been done at least twice in the literature. The first appearance was in the work by Yang *et al.* [36] wherein crazes were grown in glassy PS blends of varying ϕ and λ was measured using transmission electron microscopy (TEM). The second occurrence was by Roovers [18] who used polybutadiene blends of varying ϕ and measured plateau moduli, G_N^0, from oscillatory shear experiments in the melt (recall that G_N^0 is proportional to ν_e).

In both cases, the measured quantities had a quadratic dependence on ϕ of the form $(1-\phi)^2$. In these works though, the M_- chains were too small to significantly change the parameters a or b from zero. As we will see, when M_- is big enough to warrant nonzero a or b, these experiments will afford us a measurement of M_e which is yet to be published in the literature.

Chapter 2

Experiments

Samples were prepared using PS purchased from Polymer Source Inc. with molecular weights $M_+ = 785$ kg/mol and $M_- = 5.1$ or $M_- = 15.5$ kg/mol (weight averaged molecular weight for all cases, M_w). For the former two, the polydispersity index (PI) was 1.07 and for the latter PI was 1.04. The lot numbers, respectively, were PS-700k, P4246-S and P4247-S. Mixtures of high and low molecular weight PS were dissolved in toluene for varying weight fractions of the *low* molecular weight component, ϕ. Films ~130 nm thick were spun from solution onto freshly cleaved micah substrates and annealed for 12 h to remove residual stress and solvent. Films were then floated onto the surface of a clean water bath (Milli-Q) and picked up across a 1.5 mm gap between two fixed aluminum blocks. Together the blocks were then fastened to a single-axis translation stage, unfixed, and slowly pulled apart until

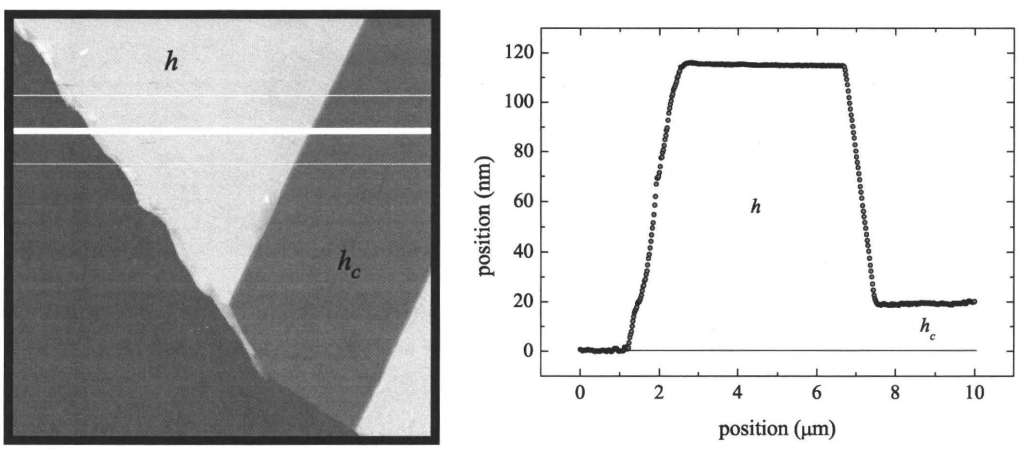

Figure 2.1: AFM image of a crazed sample showing the substrate (bottom left of image on left), crazes, h_c and undeformed polymer, h. The height profile on the right is taken from the averaged data of the white box and heavy line on the left.

crazes were formed. A constant strain rate of $\dot{\gamma} = 2 \times 10^{-4}$ s^{-1} was used and samples were strained to about $\gamma = 0.1$. The experiments were done at room temperature which is well below $T_g \sim 90$ °C.

The samples were then measured with a Veeco-Digital Instruments Multimode AFM in tapping mode *or* with a Phillips CM-12 TEM. For the AFM measurements, the strained PS samples were transferred to a Si substrate by placing them onto the substrate and letting surface forces pull the specimens into contact with the substrate. After contact was made between the previously freestanding films and the substrate, scratches were made along the edges of the aluminum blocks, confining the crazed samples to the Si wafers. In order to measure h_c and h simultaneously as shown in Figure 2.1 which shows an AFM image of a crazed PS film, scratches were made at angles to the crazes, enabling all of the craze, undeformed material and the substrate to be captured in a single scan. The state of a typical sample after the second set of scratches have been made is shown in Figure 2.2.

Since v_f has been measured most often by TEM, samples with $M_- = 5.5$ kg/mol were prepared over (nearly) the same range as for the systems for which AFM measurements were made. In this way a direct comparison between the two methods might be made for samples prepared using the same polymer, and on the same apparatus. Strained films were transferred onto PS coated Cu TEM grids, again by placing the strained films into contact with the grids and allowing surface forces to pull the PS into contact. Using a

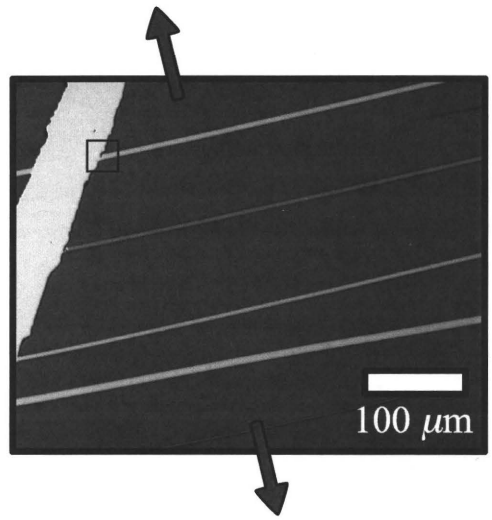

Figure 2.2: An optical microscopy image of a crazed PS sample on a Si substrate. The more horizontal lines are crazes and the thick vertical line is a scratch. The box a the top left shows where a typical AFM image might be taken, capturing all of the uncrazed and crazed material, as well as the substrate. The straining direction is indicated by the arrows. The scale bar is approximate.

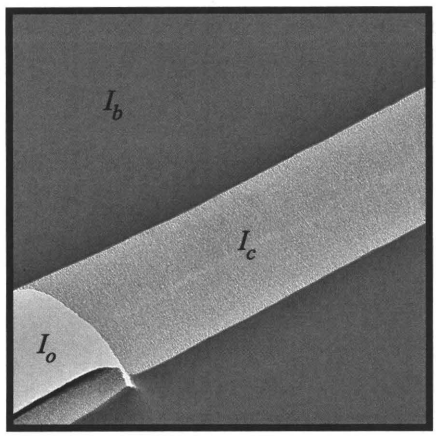

Figure 2.3: TEM image of a crazed sample showing the hole, I_o, crazes, I_c and undeformed polymer, I_b. The distance across the craze is approximately 10 μm.

focused electron beam small holes were vaporized into various portions of craze regions and a picture including the hole, craze and undeformed regions, was taken with a CCD detector; the intensities of these regions are denoted, as in Figure 1.14, I_o, I_c and I_b respectively as shown in Figure 2.3.

As we will show below, the values of λ calculated using results from these two methods were not the same for any of the ϕ used in this work. Several experiments were devised to determine whether this discrepancy was a result of differences intrinsic to the measurement techniques, or if the structure of the crazed material was somehow the reason for the discrepancy. As we will see, there is some combination of both of these ideas that is responsible for the discrepancy. Extensive calibrations of the AFM have been carried out as well as several experiments verifying that the AFM measurements are valid. Because the details of these experiments and the comparison to TEM detract from the focus of this thesis, this discussion appears in Appendix B.

I Atomic force microscopy

Atomic force microscopy is a *relatively* new technique (the first AFM was built in the mid 1980's [38]) for surface measurement that allows one to measure, in particular, height profiles of specimens in which the surface topography has height variations of about 10 μm or less over a lateral range of about 150 μm or less. In all cases discussed here, heights range from about 10-20 nm to about 100-160 nm in a typical scan area that is something like 10×10 μm^2.

The AFM paradigm is a classic vinyl record player: a sharp tip scans along a line and interacts with the surface to transmit a signal as a function of surface quality as shown in

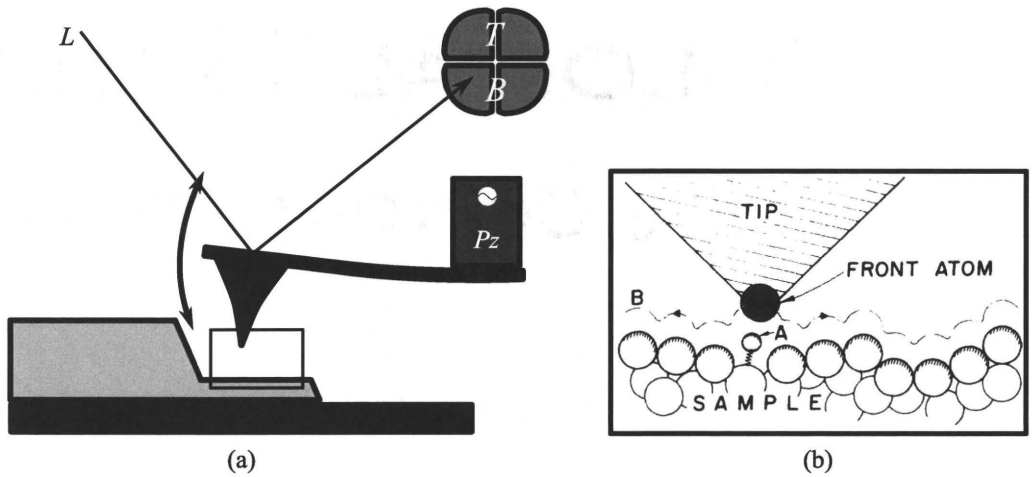

Figure 2.4: (a) the basic atomic force microscope: a piezoelectric crystal (Pz) oscillates the AFM tip at some frequency ω_o. A laser beam, L, bounces off the top of the tip and shines onto a split photodiode array, T and B, which is used to measure how much the tip is oscillating. As taken from [38] (b) shows the atoms of the AFM tip interacting with an atom on the surface of a sample, as highlighted by the boxed region in (a).

Figure 2.4. Where the record player responds to height differences, the AFM may measure changes in height, electric or magnetic field, density, etc [39]. Determining surface topography amounts to measuring the deflection of a needle-like cantilever. Early AFMs used the principles of scanning tunneling microscopes [38, 39] to measure this deflection, but in recent versions of the instrument it is more common to use a reflected laser beam to measure the deflection.

If the AFM tip can be described as a Hookean spring, then the differential equation governing its motion will be

$$m\ddot{z} + \alpha\dot{z} + kz = f_o \sin(\omega_o t) - Q(z). \tag{2.1}$$

The left hand side of this equation is just a damped simple harmonic oscillator, and the right hand side describes the external forcing. The first term on the RHS is the piezoelectric driving force and $Q(z)$ describes the interaction between the tip and the sample. When the tip is far from the surface of the sample, Q is small, but attractive. As the tip approaches the surface though, the interaction will become repulsive as the tip is embedded into the sample.

Given the form of Equation 2.1, it is possible to show that the steady state solutions, $z_s(t)$, will be periodic with frequency ω_o, but that they need not be harmonic. In free air with the AFM tip far from the surface the interaction, Q, will be negligible. In this case, the root-mean-square (RMS) amplitude of the tip's oscillation, A_f, will be relatively large.

As the sample is approached though, some of the tip's energy is transferred into the sample and the tip's oscillation amplitude will be less than A_f.

In tapping mode AFM, the cantilever tip is driven to oscillate by a piezoelectric crystal as in Figure 2.4(a) near its resonant frequency. For the experiments reported here, this frequency is something like $\omega_o = 300$ kHz. A laser is shone onto the top of the cantilever and the reflected light is collected by a 2×2 photodiode array. The purpose of the diode array is to allow calculation of the difference between the currents resulting from light incident on the top, T, and bottom, B, diodes. The horizontal splitting aids in beam alignment. The magnitude of the difference, $|T - B|$, will oscillate at the same frequency as the driving frequency and will have some root-mean-square value, in free air the value is A_f.

To measure surface topography, the oscillating tip is lowered toward the surface until the measured RMS amplitude is some user defined value $A_o = \epsilon A_f$ where $0 < \epsilon < 1$. It is the job of a set of feedback electronics to ensure that this oscillation amplitude remains as constant as possible for the duration of the data collection. Once this 'contact' with the surface has been made, the sample begins to raster in the x- and y-directions (as defined in Figure 1.11) by two other piezoelectric crystals (not shown in Figure 2.4). As the tip approaches a change in the height of the sample, as shown in Figure 2.4(a), the interaction between it and the sample changes, and this results in a change in the RMS $A = |T - B|$.

In addition to the sinusoidal driving applied to Pz of Figure 2.4(a), it is possible to apply a bias voltage, B, to regulate the mean height of the AFM tip. Changing this voltage is the job of the aforementioned feedback electronics, and their purpose is to keep the operating amplitude, A_o as constant as possible. To do this, a PID controller is used (P.I.D. stands for Proportional, Integral and Derivative). The principal of operation of a PID control is to correct the error signal $e(t)$ (here defined as $e(t) = A_o(t) - A(t)$) by considering the current value of $P = e$, how much error has accrued over some previous time period ($I = \int_{-\tau}^{0} e(t)\, dt$) and how much the error is changing ($D = de/dt$). Depending on the weighting of each of these terms, the output bias B is changed such that $B_{new} = (\kappa_P P + \kappa_I I + \kappa D)B_{old}$.

Summarizing, B is the bias voltage applied to the oscillating AFM tip. In tapping mode AFM, one wishes to maintain a constant tapping amplitude, but when the height of the sample varies, the interaction, Q, between tip and sample changes and the tapping amplitude deviates from A_o. Using PID control allows the B to be changed such that $A_o - A$ is minimized. Thus, after a calibration of B with respect to height, one can collect a spectrum of the bias voltage as a function of position, $B(x, y)$, and easily convert this data to a height spectrum, $z(x, y)$.

II Transmission electron microscopy

This technique makes use of the fact that an electron, when interacting with an atom, may scatter away from its original trajectory. A sample is illuminated from above with a beam of electrons with parallel trajectories. As the electrons interact with the sample, they will be scattered to varying degrees depending on the local sample thickness (areal density) or elemental composition. Variation in these qualities can be seen with a resolution of 1 nm or less [40].

A TEM consists of an electron gun, electron lenses and apertures, the sample and the image screen. For details outside of the sketch that follows refer to Reimer [40]. The electron gun consists of an anode and cathode and a so-called Wehnelt electrode is placed between them. Their configuration in a typical TEM is shown in Figure 2.5 and they are rotationally symmetric. A negative bias, $-U$, is applied to the cathode and a slightly more negative bias, $-(U + U_w)$, is applied to the Wehnelt electrode, while the anode is maintained at ground potential.

For the instrument used in these experiments, the cathode is made from LaB_6. Electrons are generated in a process called thermionic emission whereby the cathode temperature is raised until electrons are essentially boiled off. Raising the temperature of a metal causes the Fermi distribution function to become broadened. As such, the higher the temperature is raised, the more likely it is that an electron in the cathode will have enough energy to escape the confines of the cathode's work function. For LaB_6 cathodes, the required temperatures are roughly 1400-2000 K.

Once an electron is free of the cathode it is subject to the constraints of the electric field that is set up by the three electrodes that make up the gun. In the absence of the Wehnelt electrode, electrons exiting the cathode off the z-axis have no forces to push them back on axis. Possible trajectories are shown as dotted lines in Figure 2.5. However, since

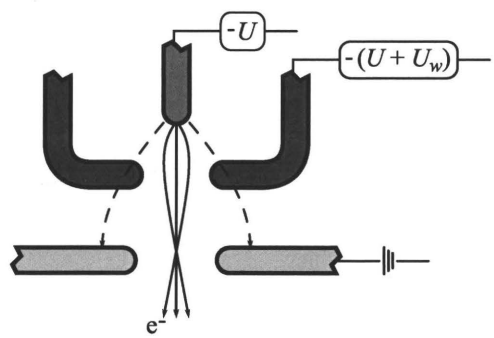

Figure 2.5: A TEM electron gun with its (top) cathode, (middle) Wehnelt electrode and (bottom) anode. Respectively, they are held at potentials $-U$, $-(U + U_w)$ and 0.

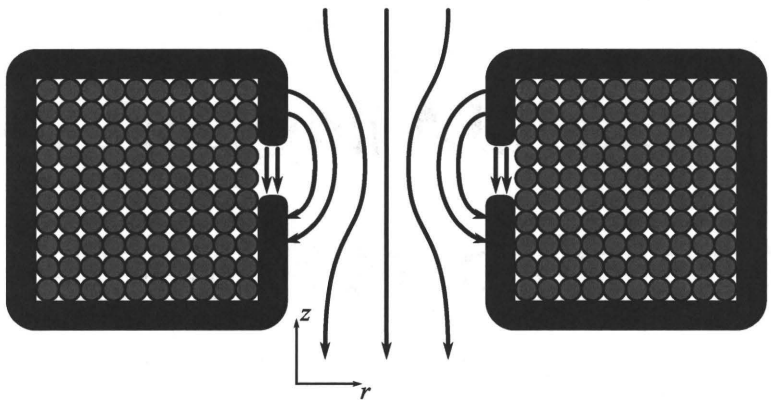

Figure 2.6: A TEM electron lens. The heavy black squares are iron pole pieces and the grey circles are coils of wire through which some current flows. The arrows represent resulting magnetic field lines.

the Wehnelt electrode is at a *lower* potential than the cathode, electrons are driven away from it and back on-axis as indicated by the curved, solid trajectories.

Even if the electrons are pushed back on-axis by the Wehnelt electrode, the electron trajectories exiting the gun are not parallel. Since it is desired that the trajectories of electrons incident on the sample in the TEM are parallel (and normal to the sample plane) some method of selecting these electrons is necessary. Furthermore, once the electrons have interacted with the sample (in regions that are of order 1 μm to smaller than 100 nm), the exiting electrons must be projected onto a fluorescent screen or CCD, the former being of order 10 cm in diameter. Redirecting and projecting electrons is done with the help of magnetic lenses, and the construction of one is shown in Figure 2.6.

In a magnetic lens, the electrons ejected from the gun are passed through a coil of wire. The coil is enveloped by a layer of iron except for a slit where there is none; the current in the coil magnetizes the iron covering. In this situation, the magnetic field is no longer isotropic in the z direction as it would be if there were no iron covering. The resulting magnetic field lines, which are a combination of the fields due to the current running through the coil and also the field due to the magnetization in the iron layer, are shown in Figure 2.6. The strength of the magnetic field in the z-direction as a function of distance, z, from the middle of the slit can be well approximated by [40]

$$B_z = \frac{B_o}{1 + \left(\frac{z}{a}\right)^2}, \tag{2.2}$$

where B_o and a are both constants. By solving the equations of motion for an electron in this field it can be shown [40], for electrons passing near the center of the coils, that the behaviour of electrons entering such an apparatus is similar to that of light passing through

a typical optical lens. That is, an electron passing through the point (r_o, z_o) on one side of the lens will pass through a point (r_1, z_1) commensurate with the modified optical equations

$$\begin{aligned} r_o &= M r_1, \\ Z_o Z_1 &= f_o f_1. \end{aligned} \tag{2.3}$$

Relating to previous convention, $r^2 = x^2 + y^2$. In the first of these equations, M is a magnification and is a function of z_o and z_1, but not of r_o or r_1. The second equation is a form of Newton's lens equation, where f_o and f_1 are focal lengths, and the variables on the left hand side are actually *functions* of z_o and z_1. The variables Z_o, Z_1, f_o, f_1 and M are also functions of the field strength and width, B_o and a, as well as the electron gun accelerating voltage, U, and the electron rest mass energy, $m_e c^2$.

In a typical TEM, there are several of these lenses. The first set is designed to ensure that all the electrons interact with the sample at right angles. This has the obvious advantage that it is much easier to model scattering results if one can assume that all incoming electrons are moving in the same direction. The second set of lenses is designed to amplify the image of scattered electrons onto a fluorescent image plate or CCD. Obviously, the functions of the two sets of lenses are different, but by tuning the strengths of B_o (by adjusting the current in the wires, say) and a (by adjusting the size of the slit in the iron coil covers) relative to the electron gun energy, U, the desired lens effect can be obtained. Actually, the parameters that control the function of the lens are a and the quantity $\omega = \sqrt{1 + k^2}$ where [40]

$$\begin{aligned} k^2 &= \frac{e B_o^2 a^2}{8 m_e \tilde{U}}, \\ \tilde{U} &= U\left(1 + \frac{eU}{2 m_e c^2}\right). \end{aligned} \tag{2.4}$$

Chapter 3

Results and discussion

As pointed out in Section V of Chapter 1, a system of polymers that is composed of long chains that are diluted with shorter chains should have the effect of reducing the the number of entanglements that sustain network stress. It was also discussed that the ratio of the heights of the crazed and uncrazed films is a function of the entanglement density (recall Equations 1.20, 1.22 and 1.27).

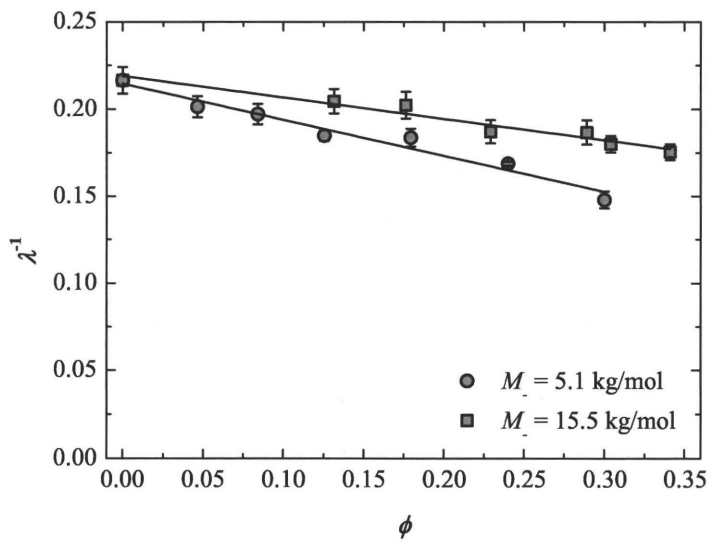

Figure 3.1: $\lambda^{-1} = h_c/h$ as a function of ϕ for $M_- = 5.1$ kg/mol and $M_- = 15.5$ kg/mol. The solid lines are fits to guide the eye.

I Varying M_-

The data presented in Figure 3.1 show the trend in λ^{-1} for $0 < \phi < 0.30$ for $M_- = 5.1$ kg/mol as well as for $M_- = 15.5$ kg/mol. Figure 3.2 shows the same data (this time squared since $\lambda^{-2} = \left(\frac{h_c}{h}\right)^2 \sim \nu_{eff}$) along with the data for $M_- = 15.5$ kg/mol over a similar range. As previously discussed ϕ measures the number of short chains in the system, and as the number of short chains increases, we expect that some of the entanglements in the system will be rendered ineffective in their role of sustaining stress, recall Figure 1.16. The way in which ν_{eff} is expected to decrease is given by Equation 1.27: if $(h_c/h)^2$ is plotted over a range of ϕ, the height ratio should decrease quadratically with ϕ. In terms of the entanglement network, we can consider that as the number of short chains is increased, the entanglement points become more widely separated, therefore we expect the system to stretch farther before being maximally extended. Furthermore, when the length of the short chains is varied, we expect that if the length is small compared to M_e, the extent to which the effective entanglement density[1], ν_{eff}, is reduced will be greater than when M_- is comparable in size to M_e.

Inspection of Figure 3.2 shows that this is indeed the case, since for $M_- = 15.5$ kg/mol,

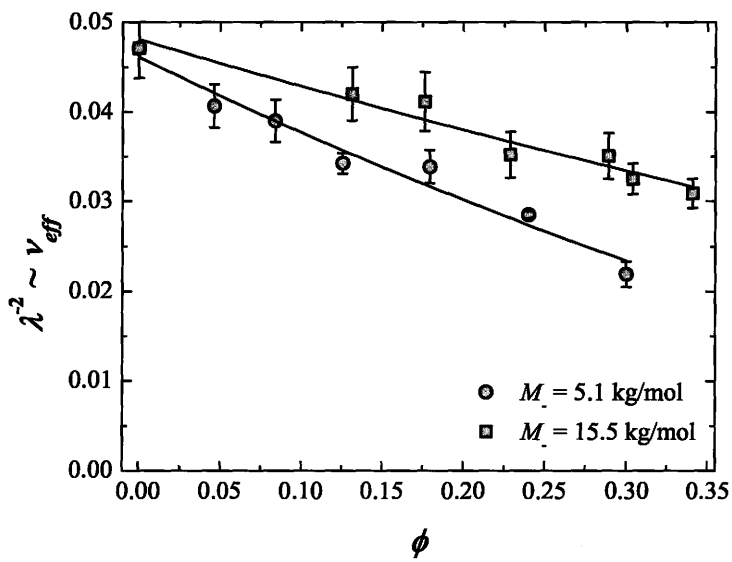

Figure 3.2: As obtained by AFM, the height ratios $\lambda^{-2} = (h_c/h)^2 \sim \nu_{eff}$. The solid lines are fits to Equation 1.27. For $M_- = 5.1$ kg/mol, $b = 0$ was imposed while for $M_- = 15.5$ kg/mol, $b = a^2$ was imposed.

[1]Recall that the *effective* entanglement density, ν_{eff}, counts only those entanglements that transmit stress across the network.

ν_{eff} is greater than that in the $M_- = 5.1$ kg/mol systems for all ϕ (except for when $\phi = 0$). We can interpret this trend in terms of an effective entanglement molecular weight, M_{eff}, by saying that when a system composed of long chains, M_+, is diluted with chains that have small molecular weights, M_-, the observed extension ratio is such as that which would be observed in a system that has a *larger* entanglement molecular weight.

i The parameters a and b

In Equation 1.26 it was stated that the ν_{eff} should have a quadratic dependence on the mass fraction of short chains as

$$\nu_{eff} = \nu_e \left[(1-\phi)^2 + 2a\phi(1-\phi) + b\phi^2\right].$$

In this expression, we assume that all the interactions between two big chains that would generally lead to entanglement still do upon the addition of short chains to the system. The parameters a and b describe the interactions between $+-$ or $-+$ and $--$ chains respectively. They must both be less than 1, and they reflect the fact that not all interactions between short chains and some other chain will lead to entanglement. For longer chains, such as the $M_- = 15.5$ kg/mol, a and b will be bigger than for when $M_- = 5.1$ kg/mol because, as will be shown below, longer chains entangle more often than short chains. It is apparent that a and b should be functions of both M_e and M_-. Here, by 'entanglement,' we refer to those interactions which, for example, lead to stress transfer between chains.

As a special case, consider when $a = b = 1$ as happens when $M_- \gg M_e$. For this case, the term above in square brackets is equal to one upon expansion. This should be expected since when all chains have $M \gg M_e$ we expect all the interactions to lead to entanglement. ν_{eff} does not change with ϕ because there is no loss of the network's ability to transfer stress. On the other hand when $a = b = 0$ (which is equivalent to saying that $+-$, $-+$, or $--$ interactions *do not* contribute to the integrity of the network), as would be the case when $M_- \ll M_e$, ν_{eff} would depend only on the entanglement density of the material, and on ϕ as $\nu_{eff} = \nu_e(1-\phi)^2$. This was the assumption made by Yang *et al.* and Roovers[36, 18] when they diluted well entangled (PS for the former, polybutadiene in the case of the latter) networks with low molecular weight chains, and they observed the expected dependence. Unfortunately, when $a = b = 0$, these types of experiments preclude a measurement of the entanglement molecular weight, M_e, as we will show below.

First though, it is prudent to comment on the relationship between the two parameters. In what follows, we will argue that a is the fraction of short chains that are entangled. In the second term of Equation 1.26, $a\phi$ is the probability that a short chain is entangled, and we multiply this by $(1-\phi)$ to give the probability that the short chain is entangled

with a long chain. Since all of the long chains are entangled, there is no prefactor for the $(1-\phi)$ terms. In the third term, we wish to count all the interactions between small chains *that are entangled.* Since, as before, the probability that a small chain is entangled is a, the probability that two small chains interact *and* become entangled is $(a\phi)(a\phi) = a^2\phi^2$. Therefore, it must be that

$$b = a^2. \tag{3.1}$$

Now, we ask how big is a? Since we consider that the entanglements that contribute to ν_{eff} are the ones that are between two *different* chains (ie, self entanglements do not count [4]), we believe the chains that are interacting with more other chains are the ones most likely to entangle. To have a high probability of getting an entanglement, a chain needs to be interacting with a sufficient number of other chains.

When the pervaded volume, V_p, of a chain is large, there are more other chains entering into V_p and interacting with it. Thus we conclude that the short chains, with molecular weight M_-, who have a prescribed minimum V_p will be the ones contributing to ν_{eff}. If a chain of some polymer species has a given molecular weight, the only way for its V_p to increase is for its end-to-end distance to increase, thus we need to consider the chains whose end-to-end distance, R, is a minimum, R_{min} or greater:

$$R \geq R_{min} \Rightarrow \text{chain contributes to } \nu_{eff}.$$

But what is the minimum end-to-end distance, R_{min}, such that V_p is big enough to allow enough other chains in, leading to entanglement? In fact, this question leads us to a new definition of M_e. We say that M_e is the molecular weight for which the pervaded volume is big enough to lead to entanglement, just as Fetters *et al.* did [6]. We use this molecular weight to define R_{min} by invoking Gaussian statistics for the chains:

$$R_{min} = \sqrt{\beta M_e} \tag{3.2}$$

The portion of chains that are longer than R_{min} is, again, determined by invoking the Gaussian probability distribution for lengths of the random walking chain. We have already discussed that this distribution is given by $\rho(R) = \left(\frac{\alpha}{\pi}\right)^{3/2} e^{-\alpha R^2}$ and α is related to chain variables by $\alpha = 3/2\beta M$ (see Equation 1.5). The probability that a chain has $R \geq \sqrt{\beta M_e}$ is given by integrating the probability distribution function over all R that satisfy this

condition:

$$\begin{aligned} P(R \geq \sqrt{\beta M_e}) &= \int_{R_{min}}^{\infty} \rho(R)\, d^3r, \\ &= 4\pi \left(\frac{3}{2\pi\beta M_-}\right)^{\frac{3}{2}} \int_{\sqrt{\beta M_e}}^{\infty} R^2 \exp\left(\frac{-3R^2}{2\beta M_-}\right) dR. \end{aligned} \tag{3.3}$$

A geometrical interpretation of this integral can be made here. Figure 3.3 shows the integrand, $\Pi = 4\pi \left(\frac{3}{2\pi\beta M_-}\right)^{\frac{3}{2}} R^2 \exp\left(\frac{-3R^2}{2\beta M_-}\right)$ as a function of R for several molecular weights. Based on the value of M_e for PS found in [6], $M_- = 0.4M_e$ and $M_- = 1.2M_e$ roughly correspond to the values of M_- used in the experiments reported here. The solid vertical line represents the end-to-end distance of an entanglement strand. The value of P for a given molecular weight is just the area under its curve to the right of the solid vertical line. As seen in the graph, when M is increased, its probability distribution function is progressively broadened and its peak shifts to the right. Because of this, as the molecular weight is increased there is progressively more and more area under the curve to the right of the solid line, and the probability that a chain's end-to-end distance is greater than the entanglement strand's gets bigger and bigger.

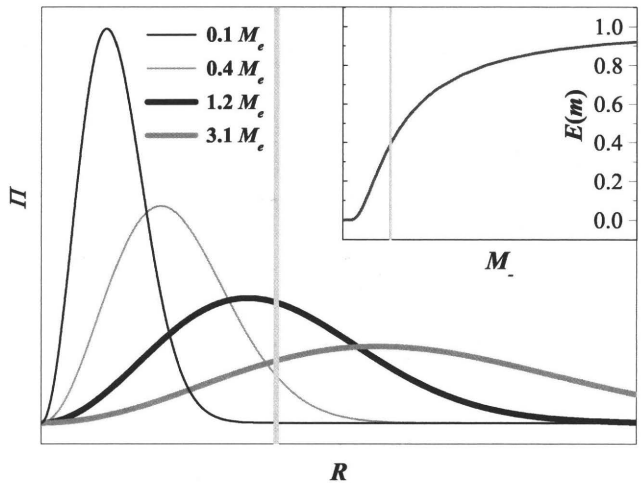

Figure 3.3: Π as a function of R for several molecular weights of PS. The light gray vertical line is $\langle R^2 \rangle^{\frac{1}{2}}$ for an entanglement strand. The inset shows the function $E(m)$ defined in Equation 3.5 for $0 < M_- < 7M_e$; the light gray vertical line shows $M_- = M_e$ and the value of $E(m)$ there is approximately 0.39.

To make Equation 3.3 somewhat more elegant, we make the change of variables $u = \sqrt{\frac{3}{2\beta M_e}}R$. Doing so, we find that $dR = \sqrt{\frac{3}{2\beta M_e}}du$ and $R = \sqrt{\beta M_e} \Rightarrow u = \sqrt{\frac{3M_e}{2M_-}}$ so that the above probability becomes

$$P(R \geq \sqrt{\beta M_e}) = \frac{4}{\sqrt{\pi}} \int_{\frac{1}{\sqrt{m}}}^{\infty} u^2 e^{-u^2}\, du \equiv E(m), \tag{3.4}$$

where $m = \frac{2M_-}{3M_e}$ can be thought of as a reduced molecular weight. In terms of polymer chains, when $M_- \to 0$, the lower integration limit in Equation 3.5 goes to infinity and $E(m)$ goes to zero[2]; there are no chains with small molecular weights that are longer than an entanglement strand. If M_- is large compared to M_e then the lower integration limit of $E(m)$ goes to zero and, since it is normalized, $E(m) \to 1$; all chains with $M_- \gg M_e$ have an end-to-end distance which is greater than that of an entanglement strand. We also note that $E(m)$ is a function of M_e and M_- only, and does not depend on the value of the β that was introduced in Equation 1.1. $E(m)$ is shown in the inset of Figure 3.3 for molecular weights $M_- \leq M_e < 7M_e$ and M_e is again indicated by the solid vertical line.

In this work, we make the claim

$$a = E(m), \tag{3.5}$$

and test this prediction with the results obtained from fitting the data in Figure 3.2 by comparing the value of M_e determined to the value obtained by Fetters *et al.* [6] in oscillatory shear experiments. When fitting the data for both $M_- = 5.1$ kg/mol and 15.5 kg/mol, we have imposed $b = a^2$ as discussed above. With the fitted value of a, we then solve for M_e with the equation

$$a = \frac{4}{\sqrt{\pi}} \int_{\sqrt{\frac{3M_e}{2M_-}}}^{\infty} u^2 e^{-u^2}\, du. \tag{3.6}$$

The method by which this equation is solved can in principal be used to any desired degree of accuracy, even though, admittedly, its spirit lies in the brute force regime of analysis. Using a computer algebra system, Maple 9.5 in this case, the function $f(m) = a - E(m)$ is plotted over a large enough range to find the m-intercept. The plotting range is then reduced making sure to leave the intercept in the plotting range until the desired numerical accuracy in the range is obtained. For a given value of a, the m-intercept, m_a, is then taken to be

$$m_a = \frac{2M_-}{3M_e}, \tag{3.7}$$

which can easily be solved to give a numerical value for M_e since M_- is an experimentally

[2] If we make the substitution $x = 1/\sqrt{m}$ then $E(x)$ can be related to the complementary error function, erfc(x) by

$$E(x) = \frac{2x}{\sqrt{\pi}} e^{-x^2} + \text{erfc}(x).$$

controlled parameter and m_a is found as described above.

In the case of $M_- = 5.1$ kg/mol, the result of fitting gives $a^{(5.1)} = 0.04 \pm 0.07$. This indicates that about 4% of the interactions between short chains and long chains result in entanglements. Although the error in the fit is large ($a^{(5.1)}$ can be said to be equal to zero within error), we can still try to gain insight by finding the value of M_e which satisfies Equations 3.6 and 3.7. Doing so we find that

$$M_e^{(5.1)} = 14.1 \text{ kg/mol.} \qquad \text{(PS)}$$

Using the upper bound found in the fit, $a_{max}^{(5.1)} = 0.11$, one can place a lower bound on the value for M_e using the same method, and this results in $M_{e,\,min}^{(5.1)} = 10.3$ kg/mol. Similarly, we can compute an upper bound for M_e as determined from the $M_- = 5.1$ kg/mol data. The lower bound of $a^{(5.1)}$ is $a_{min}^{(5.1)} = 0$ (since it cannot be less than 0). Substituting $a = 0$ in Equation 3.6 gives, in a disappointingly unenlightening manner, $M_{e,\,max}^{(5.1)} = \infty$. Fortunately, the $M_- = 15.5$ kg/mol data will provide us with a more meaningful upper bound.

For $M_- = 15.5$ kg/mol, the result of fitting is $a^{(15.5)} = 0.44 \pm 0.05$ which gives $b = a^2 = 0.19$. This tells us that about 44% of the interactions between short chains and big chains result in entanglement, while only about 19% of the interactions between short chains and short chains result in entanglement (at least as far as crazing is concerned). Satisfying Equations 3.6 and 3.7 using $a^{(15.5)} = 0.44$ this time requires that

$$M_e^{(15.5)} = 14.0 \pm 1.5 \text{ kg/mol,} \qquad \text{(PS)}$$

where again the error was found by taking the extreme values allowed by the fitting. These results for M_e are comforting in light of the fact that M_e for PS reported in [6] is about 13 kg/mol.

A useful check of this model is provided by the data presented in [18] which is shown in Figure 3.4. There, polybutadiene (PBD) melts were subjected to oscillatory shear experiments of the type described in Section III.iv of Chapter 1. The melts were mixtures of high molecular weight chains and were diluted with some low molecular weight chains, $M_- = 1.8$ kg/mol. The mixtures were prepared with $0 \leq \phi \leq 0.838$ (a much broader range than for the experiments presented here) and for each melt the plateau modulus, G_N^0, was measured.

As seen in Figure 3.4, the data for G_N^0 as a function of ϕ is fit well by a quadratic of the form given by Equation 1.27. Where in that equation, the prefactor is the square extension ratio for $\phi = 0$, $\lambda_o^{-2} \sim \nu_e$, the prefactor in this case is G_N^0 which we recall is also proportional to ν_e as given by Equations 1.13 and the reciprocity of M_e and ν_e. The fact that the fit seems to be so good here is, in hindsight, reassuring since while the data presented in Figure 3.2 is well fit by a quadratic function, may also be fit by a linear function if we did not

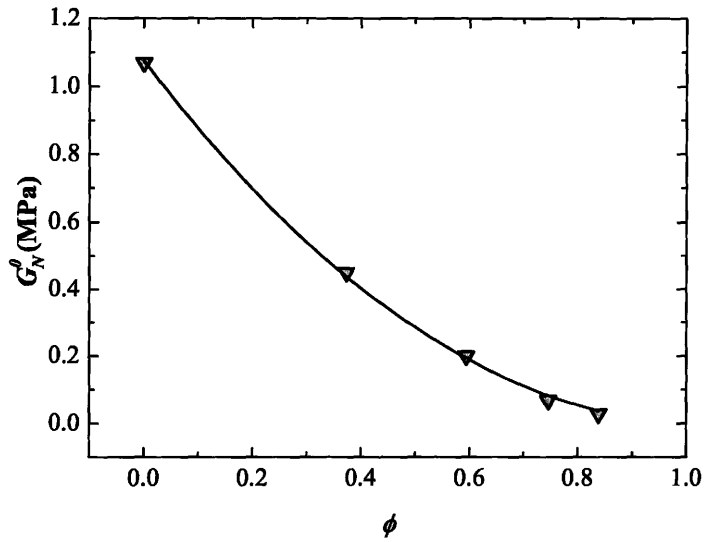

Figure 3.4: Roovers's [18] oscillatory shear results for G_N^0 as a function of ϕ. The solid line is a best fit to a modified version of Equation 1.27, where the prefactor is just G_N^0 for an undiluted system.

believe the model captured by Equation 1.27.

When fit to Equation 1.27, the data in Figure 3.4 yields $a = 0.03 \pm 0.01$. Performing the same analysis as above for the PS samples, this leads us to

$$M_e^{(1.8)} = 5.4 \pm 0.8 \text{ kg/mol.} \qquad \text{(PBD)}$$

There are various species of PBD, each of them with a slightly different M_e as reported in [6]. There, M_e was obtained again through the use of oscillatory shear experiments. For our purposes, we can say that the value reported there was roughly $M_e = 1.8$ kg/mol, exactly the same as M_- used in the Roovers experiments. If this were the true value of M_e, our analysis predicts that a here should have been about 0.4. If we also believe that $b = a^2$ then in this case we should see the graph[3] in Figure 3.4 go through 1.07 MPa$\times [0.4^2] = 0.17$ MPa when $\phi = 1$. However, when $\phi = 0.838$, G_N^0 has already fallen to 0.028 MPa, so based on our model, it seems unlikely that $M_e = 1.8$ kg/mol. M_e for PBD was obtained [41] by measuring nuclear magnetic resonance spectra in deuterated specimens and inferring chain relaxation times from the spectra. Their models relate the relaxation time spectra to M_e

[3]The parameter b in Equation 1.27 essentially describes the behaviour of ν_{eff} at $\phi = 1$. When $\phi = 1$, only the last term there survives and we have $\nu_{eff} = 1.07a^2 = 0.17$.

and for this parameter they obtained 5.380 kg/mol which is in agreement with the values we have found above.

It appears that a crossroads has been reached at this point. On one hand, we have presented new results that indicate support for the model of Fetters *et al.* since the values of M_e predicted by our model, encompassed by Equations 1.27, 3.1 and 3.5, agree with their packing model (which seems to have garnered continued support) and oscillatory shear experiments. However, in the case of Roovers's shear experiments, we find disagreement in the values predicted by our model and theirs. Some insight can possibly be gained by considering the results of our experiments when $M_- = 5.1$ kg/mol, or according to Figure 3.3, $M_- = 0.4\, M_e$. In that case, the agreement between our measured M_e and that measured in Fetters *et al.*, depending on the value of a one believes from our experiments, may not have been so good. From the limited sampling we have made here, it appears that agreement between our models might depend on M_- in the sense that it should be chosen such that a differs significantly from 0.

ii Denouement

If one believes our model, I will leave this thesis with a final remark before concluding. In what has been described so far, we have always made the assumption that $M_+ \gg M_e$ but this need not be the case. In fact, a robust test of our model could be a measurement of M_e, as described above, using bimodal molecular weight systems of polymers in which neither of M_+ or M_- are much greater than M_e. For the experiment to work though, one must see some change in ν_{eff} as a function of ϕ (which again measures the number of smaller chains in the system), so the two should be sufficiently different from one another. In this system, we can define a_+ and a_- where

$$\begin{aligned} a_\pm &= E(m_\pm) = \frac{4}{\sqrt{\pi}} \int_{\frac{1}{\sqrt{m_\pm}}}^{\infty} u^2 e^{-u^2}\, du, \\ m_\pm &= \frac{2M_\pm}{3M_e}. \end{aligned} \tag{3.8}$$

The former quantity describes the number of $++$ interactions that contribute to the entanglement density and the latter describes the $--$ interactions. In this system the effective entanglement density, if it obeyed our model, would vary with ϕ as

$$\nu_{eff} = \nu_e \left[a_+ a_+ (1-\phi)^2 + 2a_+ a_- \phi(1-\phi) + a_- a_- \phi^2 \right]. \tag{3.9}$$

Actually, this recipe can be generalized to mixtures of any number of molecular weights by considering all binary interactions between chains of different molecular weights

$$\nu_{eff} = \nu_e \sum_i^{\tilde{N}} \sum_j^{\tilde{N}} a_i a_j \phi_j \phi_i, \tag{3.10}$$

where $\tilde{N}$ is the number of different molecular weights, M_i, that make up the system and the obvious normalization constraint is

$$1 = \sum_i^{\tilde{N}} \phi_i. \tag{3.11}$$

Since we have arrived at a general expression for discrete systems of polymers, it makes sense to generalize this to *continuous* distributions of polymer molecular weights. In this regime, the ϕ_i in Equation 3.11 take on a continuous distributions $\phi_c(M)$ and the sums become integrals over all molecular weights, M,

$$\begin{aligned} \nu_{eff} &= \nu_e \iint a(M_1)a(M_2)\phi_c(M_1)\phi_c(M_2)\, dM_1 dM_2, \\ 1 &= \int \phi_c(M)\, dM, \end{aligned} \tag{3.12}$$

where the limits of integration are 0 and ∞ for all cases, and within the framework of our model, $a(M_i)$ are still given by Equation 3.8.

II Conclusion

We have introduced the idea that the addition of some short chains to a system of long chains might reduce its effective entanglement density, ν_{eff}. A model for the reduction in entanglement is proposed that asserts entanglements are the result of binary interactions between chains and that binary contacts can be treated independently. We say that all the interactions between two long chains contribute to the entanglement density. However, when M_- is not much larger than M_e some of the interactions between chains that would have resulted in entanglement, were both chains long compared to M_e, will not contribute to ν_{eff}.

In the spirit of the Fetters packing model, we attempt to predict the reduction in ν_{eff} as short chains are added to the systems. Our model stipulates chains that have an end-to-end distance which is greater than the same measure for an entanglement strand are the ones that contribute to ν_{eff}. From this stipulation, we have essentially defined M_e. When we fit our data obtained from crazing and AFM experimetns with the model, the value of M_e determined agrees with values that are found in the literature. This represents a new method of measuring M_e of a given polymer. An attractive feature of this model is that

the measurements need not even be done with the use of crazing and AFM or TEM, any measurement that gives a quantity which is proportional to ν_{eff} will do.

Appendix A

An alternative to the random walk assumption

In the work concerning dilution experiments of Yang *et al.* [36], the possibility of a different scaling for the long chains in a binary mixture of chains is mentioned. They argue, on the basis of de Gennes' scaling arguments concerning one long chain in a sea of short chains [8] that it is possible for the long chains in the network to have a different scaling, in particular an entanglement strand would have a swelled undeformed length

$$d_s \sim M_e^k, \tag{A.1}$$

where $\frac{1}{2} < k < 1$. The idea applies to a long chain in a sea of short chains. If this were the case then the scaling in Equation 1.23 would be changed because of the fact that $d_s/l_e \sim M_e^{k-1}$. As a result of this new scaling, we would need to consider a modified version of Equation 1.23, that being

$$\left(\frac{h_c}{h}\right)^{\frac{1}{1-k}} \sim \nu_e, \tag{A.2}$$

so we see that it is important to have the right molecular scaling model if we are to accurately predict the entanglement density of our systems.

According to de Gennes, the effect is important when the length of the short chains is such that $N < N_+^{\frac{1}{2}}$ where N and N_+ are the number of steps in the trajectory of a chain. To clarify this statement, we say that if an *isolated* long chain is in a system that satisfies the above condition, its end-to-end distance will be dominated by an exponent different from $\frac{1}{2}$. For a polymer chain, the number of steps in its random walk, N, and its molecular weight, M, are related by $M = M_o N$ where M_o is about 0.83 kg/mol for PS [37]. Using this, we can make the condition of de Gennes one which relates the molecular weights instead of the

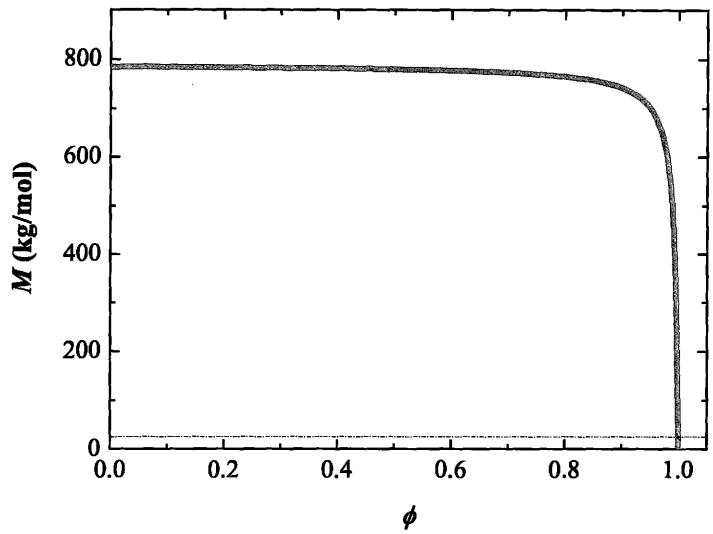

Figure A.1: Molecular weight of our diluted polymer systems as a function of ϕ (solid gray line) and the molecular weight at which the long chains begin to swell (broken horizontal line).

number of statistical walk segments for the chain

$$M < (M_o M_+)^{\frac{1}{2}}. \tag{A.3}$$

Considering the systems we have used, with $M_- = 5.1$ kg/mol (at the least) and $M_+ = 785$ kg/mol we can compute the weight averaged molecular weight of the system which is the ratio of the first and second moments of the molecular weight distribution

$$M = \frac{\sum_i n_i M_i^2}{\sum_i n_i M_i}, \tag{A.4}$$

where n_i are the numbers of chains with molecular weight M_i. In our systems, there are two M_i, M_- and M_+ and the n_i can be replaced by the weight fractions ϕ for M_- and $(1-\phi)$ for M_+. Therefore, the 'mean field' molecular weight that any given chain feels in the melts of our system are

$$M = \frac{\phi M_-^2 + (1-\phi) M_+^2}{\phi M_- + (1-\phi) M_+}. \tag{A.5}$$

Using Equations A.3 and A.5 we will see a cross over from random walking, $k = \frac{1}{2}$, to

swelled chains, $\frac{1}{2} < k \leq 1$ when

$$(M_o M_+)^{\frac{1}{2}} = \frac{\phi M_-^2 + (1-\phi) M_+^2}{\phi M_- + (1-\phi) M_+}. \tag{A.6}$$

The case of PS with M_+, M_- and M_o as quoted above is shown in Figure A.1. From this plot, it appears that even with a high degree of dilution the molecular weight for the system that a given long chain sees is still large compared to $(M_o M_+)^{\frac{1}{2}}$. Since the largest ϕ ever gets in our experiments is no bigger than $\phi_{max} \simeq 0.35$, it appears as though we need not consider this chain swelling behaviour.

Appendix B

AFM and TEM λ measurements

Figure B.1 shows the ratio of the crazed film height to its undeformed height, $h_c/h = \lambda^{-1}$, for $M_- = 5.1$ kg/mol. For both the AFM and TEM measurements, the ratio is a decreasing function of ϕ. The inset shows the ratio of the data from the two different experiments. Within experimental error, one may say that the ratio is constant and has a value of

$$\Lambda \equiv \frac{\lambda_{TEM}^{-1}}{\lambda_{AFM}^{-1}} = 1.2 \pm 0.1. \tag{B.1}$$

In this appendix, the discrepancy between AFM and TEM measurements is detailed.

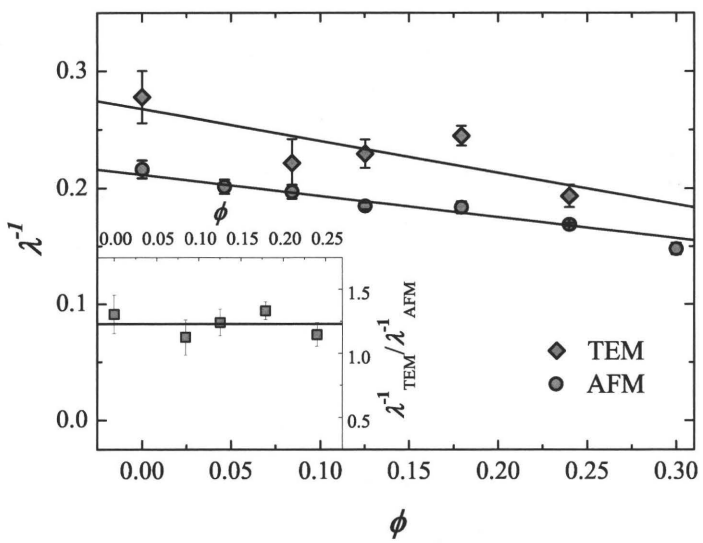

Figure B.1: $\lambda^{-1} = h_c/h$ as a function of ϕ for $M_- = 5.1$ kg/mol, the solid lines are linear fits to guide the eye. The inset shows the ratios $\lambda_{TEM}^{-1}/\lambda_{AFM}^{-1}$ as a function of ϕ. The solid line in this inset is the average value of the five data points.

Several experiments were done to determine the source of the discrepancy and we find that the it is, in large part, a result of some intrinsic differences in height measurements for each method. Since the AFM we used here was calibrated extensively, the λ's obtained from this instrument are the correct ones, as long as one takes into account the packing fraction of the craze fibrils making up the deformed regions. The conclusions drawn above are not affected by the discrepancy between the two measurements.

1 Crazes

Samples were prepared which composed of two PS films placed on a PS coated Cu TEM grid. The whole of the sample area was covered with a thin film, $h_1 \sim 20$ nm, half of which was covered with a thicker film with $h_2 \sim 100$ nm as shown in Figure B.2. Using a focussed electron beam, a small hole was burned in the 20 nm film near the edge of the 100 nm film. A TEM image was then taken capturing all of $I_o, I_{(1)}$ and $I_{(1)+(2)}$. The same film system was then transferred to a Si substrate and AFM images were taken of the films to measure both h_1 and $h_1 + h_2$. Given this data, it is then possible to measure a sort of pseudo extension ratio by applying the recipes as outlined in sections IV.ii and IV.iii of Chapter 1 to the heights and intensities measured.

While the rest of experiments outlined in the next section are all illuminating in their own right, the most definitive of them is the one in which there were two films with heights h_1 and h_2 stacked on top of one another as in Figure B.2. These experiments have shown that there is indeed a systematic difference between the heights as measured using atomic force microscopy and using the analysis methods of Kramer and Brown [25, 27] for transmission electron microscopy data, Equation 1.25.

From Figure B.3, which shows the observed values for the calculated height ratios, $\tilde{\lambda}^{-1} = h_1/(h_1 + h_2)$, plotted on a number line (vertical separations are irrevelant), we can see that the spread in measured values measured for the height ratio reflects the observed error signals found in Figure B.1. That is, the uncertainty in λ^{-1} is much greater for data calculated from TEM measurements than it is for the same type of measurement in the AFM. In addition to this fact, and the more relevant result is the fact that the calculated TEM values are

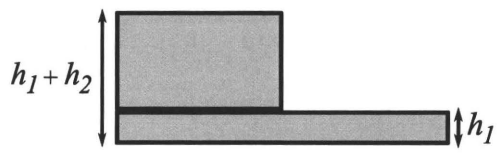

Figure B.2: The samples prepared by stacking two films with heights approximately equal to typical craze and undeformed thicknesses.

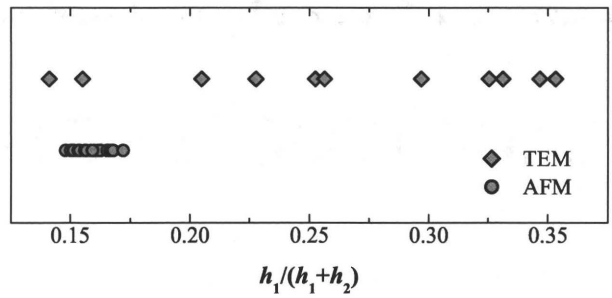

Figure B.3: $\tilde{\lambda}^{-1} = h_1/(h_1 + h_2)$ for AFM and TEM experiments. For the TEM data, the height ratios were calculated using Equation 1.25. The vertical separations between the two are irrelevant.

consistently greater than the ones obtained from AFM data.

If one takes the average of the data presented in Figure B.3, it is found that the ratio of the data from the two types of experiments is given by

$$\tilde{\Lambda} \equiv \frac{\tilde{\lambda}^{-1}_{TEM}}{\tilde{\lambda}^{-1}_{AFM}} = 1.7 \pm 0.3. \tag{B.2}$$

Based on the analysis of Kramer and Brown [25, 27] one should expect that the ratio in Equation B.2 would have turned out to be equal to 1. Since this is the not the case, we should ask which value of $\tilde{\lambda}^{-1}$ we believe: that from the AFM results or that from the TEM results. To answer this question we turn to the calibration data obtained for the AFM. As discussed below, calibration grids were used with various step heights. After analyzing the results of AFM scans, it was found that the measured heights were consistent with the manufacturer's specifications for each of the three grids. Since this is the case, we are lead to believe that the values of $\tilde{\lambda}^{-1}$ measured by AFM are the true values and that the values as calculated from TEM measurements must be off by the factor in Equation B.2.

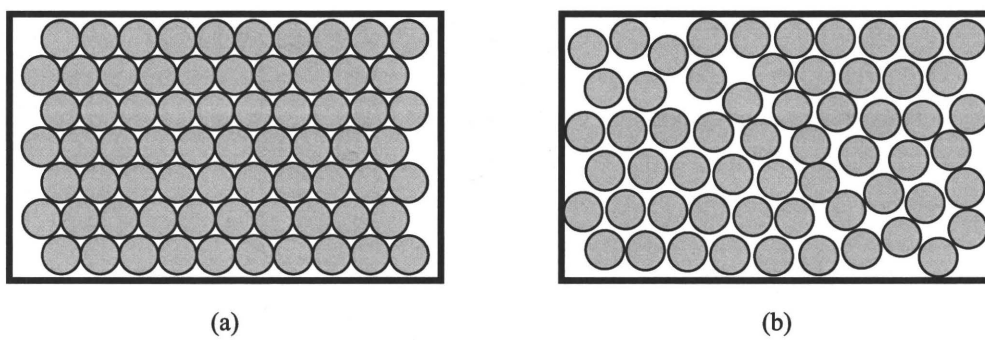

Figure B.4: Packing fractions of two arrangements of circles.

Referring to the data presented in Figure B.3 and Equation B.2, and given the results of the AFM calibration experiments, it is appropriate to scale the values of λ_{TEM}^{-1} by $\tilde{\Lambda}$. Doing so, one finds that the new ratio of the extension ratios, λ^{-1}, is

$$\Lambda_r = \frac{\lambda_{TEM}^{-1} \div \tilde{\Lambda}}{\lambda_{AFM}^{-1}} = \frac{\Lambda}{\tilde{\Lambda}} = 0.7 \pm 0.2 \tag{B.3}$$

We will now try to understand this result in terms of the structure of craze fibrils. For this purpose, we will make the simplifying assumption that for any constant x plane in a craze region (refer to Figure 1.11(b)), the fibrils can be taken to be some array of packed circles[1] of more or less constant radius. We also assume that the circles' boundaries are uncrossable. Since this is the case all space cannot be filled by the craze fibrils; there must be voids between them.

In an AFM experiment which is measuring the height profile of a sample, the internal structure of the sample does not influence the measurement to a large degree. Since this is the case, the AFM measurement alone is not capable of measuring the extent to which the material below it is filled with voids. On the other hand, the internal structure of a sample has a large influence on the results of a TEM measurement. For the case of craze fibrils, we say that the voids between the fibrils do not scatter electrons, but the material making up the fibrils does scatter electrons. Based on this argument, we expect that the measured height ratio $\lambda_{TEM}^{-1} < \lambda_{AFM}^{-1}$, and inspection of equation B.3 indeed shows this to be the case.

To understand whether the numerical value of the ratio in Equation B.3 is reasonable, we will consider the packing fractions of some circles in a plane. The densest packing of circles in the plane is given by the hexagonal lattice, as shown in Figure B.4(a), and the packing fraction is $\Lambda_h \simeq 0.91$. Based on Equation B.3 we do not expect that the packing of the craze fibrils to be hexagonal. Figure B.4(b) shows the same area as in (a) filled to a packing fraction that is $\Lambda_r = 0.7$. Given the fact that craze fibrils contain some number of defects, such as size variation and cross tie fibrils (which are bundles of polymer that connect two craze fibrils), it is perhaps reasonable to expect that the arrangement of the fibrils would give the packing fraction shown in Figure B.4(b). No attempt has been made to quantitatively predict or measure what effect size variation or cross ties would have on the packing fraction of circles, though introducing cross tie fibrils would be akin to introducing size variation in the packing images above.

[1] The argument is also valid if we consider an array of packed ellipses since the packing fraction does not depend on the radii of an ellipse.

2 Extras

1 Craze electron diffraction

One may also ask whether the structure of the observed crazes influences the scattering of incident electrons significantly by diffraction. The fibrillar structure of the crazes has a preferred length scale as opposed to the uncrazed film which is isotropic. In order to check whether the incident electrons were scattered differently by the craze structure, TEM diffraction experiments were done on both crazed and uncrazed film regions in the same sample. The results of these experiments were indistinguishable from one another. This may have been expected since the de Broglie wavelength for a 120 keV electron is about 3×10^{-3} nm and the typical length scale of a craze fibril is roughly 10's of nm.

2 Tip penetration

In tapping mode AFM, the tip is periodically in contact with the sample. When it comes down onto the sample, one may ask to what degree it penetrates into the surface. More importantly, one may ask if there is a difference between the tip-sample penetration magnitude in different areas of the sample. In the context of crazes, this could give rise to a systematic difference in measured height between the craze and uncrazed regions. This might happen because the crazes are fibrillar and, perhaps, more mobile than the surrounding undeformed material.

One method of checking to see if this effect is significant is to vary the tapping amplitude of the AFM tip and checking to see if the ratio of heights h_c/h changes significantly. We have performed experiments of this type on a $\phi = 0$ sample. The tapping amplitude set point was varied over a range of 45% to 95% of the free air tapping amplitude while the tip driving amplitude was kept constant.

To see what effect tip penetration might have on the observed height ratio, consider the case where tip penetration has the same magnitude in both the crazed and uncrazed material. If the tip sinks into the surface a distance δ, then the measured heights will be less than the real heights and the measured extension ratio will be

$$\lambda_\delta^{-1} = \frac{h_c - \delta}{h - \delta}. \tag{B.4}$$

Now we will consider the derivative of λ_δ:

$$\frac{d\lambda_\delta^{-1}}{d\delta} = -\frac{h - h_c}{(h - \delta)^2}. \tag{B.5}$$

Now, $\delta < h_c < h$, then it must be true that $d\lambda_\delta^{-1}/d\delta < 0$ for all δ. Since this is the case,

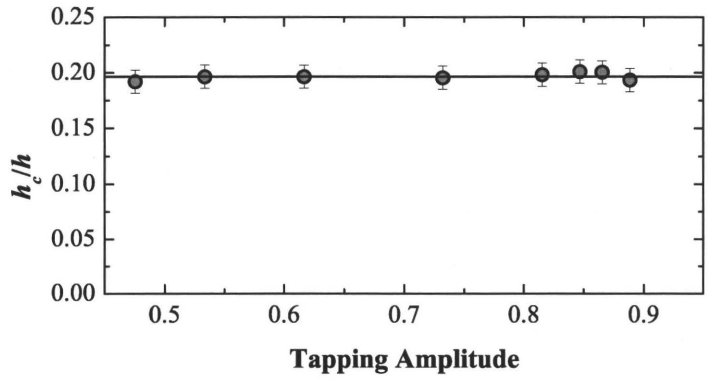

Figure B.5: The effect of the AFM tapping amplitude (in % of the free air oscillation amplitude, A_f) on the observed height ratio, λ^{-1}. The solid line is the average value of all the data and lies within the uncertainties of all the data points. The uncertainty was calculated by assuming that the measured heights had an error of 1 nm.

the effect of tip penetration has the effect of decreasing the observed λ^{-1}. This is consistent with the observed difference between λ_{TEM}^{-1} and λ_{AFM}^{-1}, however, as shown in Figure B.5, changing the tapping amplitude has no effect on the observed λ, therefore we conclude that this effect is not responsible for the difference between the TEM and AFM measurements.

3 Calibration

The model used to calculate λ from the observed TEM intensities assumes that the observed electron intensity is an exponentially decreasing function of film thickness. PS films of thickness between 20 nm and 120 nm (typical thicknesses of crazed and uncrazed films) were spun from solution onto mica and annealed for 12 h at ~25 °C above T_g. The samples were then floated onto PS coated TEM grids and TEM images of the samples were then taken. After the intensity measurements were made, the samples were then transferred onto silicon substrates and height measurements were taken with the AFM so that plots of thickness versus intensity could be built. In order to test that the AFM heights given by the analysis software were accurate, calibration grids were purchased from Mikromasch with step heights of 19 nm and 84 nm and a third grid with 180 nm steps was also used. In all cases manufacturer's quoted uncertainty in these heights was approximately 1 nm. On each grid, AFM scans were done over several steps and the average measured height was computed. In all cases, the observed height was consistent with the manufacturer's quoted value.

Figure B.6 shows the observed TEM intensity as a function of film thickness for $0 < h < 100$ nm. These experiments were done to test the validity of the exponential model for the heights we used here (refer to Equation 1.24 and [25, 35]). While the observed trend

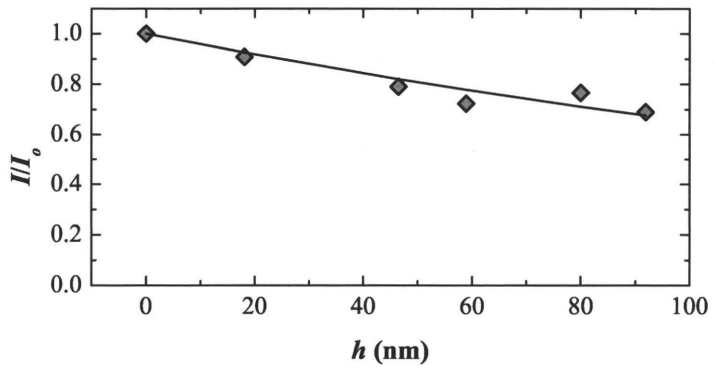

Figure B.6: Observed TEM intensity as a function of PS Film thickness. The solid line is a fit to $e^{-h/\ell}$ where h is the film thickness and ℓ is a damping coefficient. I_o is the intensity of an image with no sample in the viewing area.

in Figure B.6 is not definitively exponential, the exponential model we have used here gives a decent fit to the data. Figure 4 of Lauterwasser's work [25] shows a semilog plot of the same type of experiment. In that work, film thicknesses of up to about 1500 nm were used. At least until about $h = 1000$ nm, the plot shows that the exponential model works quite well as the data could be accurately described as a straight line in this region on the semilog plot.

As well, ℓ is essentially a measure of the mean free path of an electron in PS. Crewe and Groves [35] show a plot of the mean free path as a function of electron beam energy. In this plot, they show that the mean free path for an electron with kinetic energy $U \sim 100$ keV (here we used $U = 120$ keV) is of order 300 nm. Fitting the exponential model to the data presented in Figure B.6, one obtains $\ell = 230 \pm 30$ nm. Since this is the right order of magnitude as stated by Crewe and Groves, we believe that the exponential model is at least a good approximation to use in our interpretations of the TEM data we obtained. The fact that the data in Figure B.6 appears to be a straight line is a reflection of the fact that for the thicknesses used here the electrons have not travelled through a sufficient number of mean free paths for the exponential behaviour to be observed.

However, if the exponential model is not quite right, we can make an approximation at how wrong the exponential model has to be in order for the TEM results to be consistent with the AFM ones. Supposing that the exponential model is almost right, we can say that I_o in Equation 1.24 is now a *function* of the height. In what follows, we assume that for the crazed material, which is only 20 nm thick, the non exponential behaviour is negligible so that $I(h_c) = I_o$. We also assume that for the undeformed material, the non exponential behaviour is not negligible and that $I(h) = \varepsilon I_o$. In this case we have for the intensity of

electrons measured as hitting the viewing screen

$$\begin{aligned} I_c &= I_o e^{-\frac{h_c}{\ell}}, \\ I_b &= \varepsilon I_o e^{-\frac{h}{\ell}}. \end{aligned} \tag{B.6}$$

Before, we assumed that $I(h) = I(h_c)$, however, if this is not the case, then the calculated value of h_c/h as given in Equations 1.24 and 1.25, after a little bit of algebra, is

$$\frac{h_c}{h} = \left[1 - \frac{\ln(I_c/I_b)}{\ln(I_o/I_b)}\right]\left[1 + \frac{\ell}{h}\ln(\varepsilon)\right]. \tag{B.7}$$

If $\varepsilon = 1$, the form as given by Equation 1.25 is recovered. However, we see that if the exponential behaviour is not obeyed, serious difficulties will arise in our interpretation of the TEM results.

The measured quantities in a TEM experiment are in the first set of square brackets of Equation B.7. Also, since considerable AFM calibration has been carried out, we take the left hand side here to be given by the AFM measurements (not considering the packing fraction of the fibrils). So Equation B.7 is actually an equation which relates Λ of Equation B.1 to the variable ε which describes the degree of non exponentiality in the scattering and detection of electrons in the TEM used here. Dividing the first square bracket in Equation B.7 we find

$$\frac{\frac{h_c}{h}}{1 - \frac{\ln(I_c/I_b)}{(I_o/I_b)}} = \Lambda^{-1} = 1 + \frac{\ell}{h}\ln(\varepsilon). \tag{B.8}$$

Given that we know ℓ and h for a typical experiment, we ought to be able to solve for ε. Using $\ell = 230$ nm, $h = 130$ nm and $\Lambda^{-1} = \frac{1}{1.23} = 0.81$ we find that

$$\varepsilon = \exp(-\frac{h}{\ell}[1 - \Lambda^{-1}]) = 0.90. \tag{B.9}$$

This tells us that the exponential model of scattering *and* detection need only be 10% different between the crazed and uncrazed portions of the film to explain the differences observed in λ_{AFM}^{-1} and λ_{TEM}^{-1}.

Bibliography

[1] J. Ho, L. Govaert, and M. Utz. Plastic deformation of glassy polymers: Correlation between shear activation volume and entanglement density. *Macromolecules*, 36:7398–7404, 2003.

[2] J. Rottler and M.O. Robbins. Growth, microstructure, and failure of crazes in glassy polymers. *Physical Review E*, 68(011801):1–18, 2003.

[3] E.J. Kramer. Microscopic and molecular fundamentals of crazing. *Advances in Polymer Science*, 52/53:1–56, 1983.

[4] L. Si, M.V. Massa, K. Dalnoki-Veress, H.R. Brown, and R.A.L. Jones. Chain entanglement in thin freestanding polymer films. *Physical Review Letters*, 94:127801, 2005.

[5] P.G. de Gennes. Reptation of a polymer chain in the presence of fixed obstacles. *The Journal of Chemical Physics*, 35(7):572–579, 1971.

[6] L.J. Fetters, D.J. Lohse, D. Richter, T.A. Witten, and A. Zirkel. Connection between polymer molecular weight, density, chain dimensions, and melt viscoelastic properties. *Macromolecules*, 27(17):4639–4647, 1994.

[7] S.-Q. Wang. On chain statistics and entanglements of flexible linear polymer melts. *Macromolecules*, 40:8684–8694, 2007.

[8] P.G. de Gennes. *Scaling Concepts in Polymer Physics*. Cornell University Press, 1979.

[9] G.D. Wignall, D.G.H. Ballard, and J. Schelten. Chain conformation in molten and solid polystyrene and polyethylene by low-angle neutron scattering. *Journal of Macromolecular Science B, Physics*, B12:75–98, 1976.

[10] G.C. Berry and T.G. Fox. The viscosity of polymers and their concentrated solutions. *Advances in Polymer Science*, 5:261, 1968.

[11] A.M. Donald and E.J. Kramer. Effect of molecular entanglements on craze microstructure in glassy polymers. *Journal of Polymer Science: Polymer Physics Edition*, 20:899–909, 1982.

[12] M. Rubinstein and R.H. Colby. *Polymer Physics.* Oxford University Press, 2003.

[13] R.A.L. Jones. *Soft Condensed Matter.* Oxford University Press, 2002.

[14] J.D. Ferry. *Viscoelastic properties of polymers, 3rd ed.* John Wiley & Sons, Inc., 1980.

[15] L.J. Fetters, W.W. Graessley, and A.D. Kiss. Viscoelastic properties of polyisobutylene melts. *Macromolecules*, 24:3136–3141, 1991.

[16] J.F. Sanders, J.D. Ferry, and R.H. Valentine. Viscoelastic properties of 1,2-polyisobutylene melts – comparison with natural rubber and other elastomers. *Journal of Polymer Science: Part A-2*, 6:967–980, 1968.

[17] S. Onogi, T. Masuda, and K. Kitagawa. Rheological properties of anionic polystyrenes. i. dynamic viscoelasticity of narrow-dsitribution polystyrenes. *Macromolecules*, 3(2):109–116, 1970.

[18] J. Roovers. Linear viscoelastic properties of polybutadiene. A comparison with molecular theories. *Polymer Journal*, 18(2):153–162, 1986.

[19] J.M. Carella, W.W. Graessley, and L.J. Fetters. Effects of chain microstructure on the viscoelastic properties of linear polymer melts: Polybutadienes and hydrogenated polybutadienes. *Macromolecules*, 17:2775–2786, 1984.

[20] C. Liu, J. Jiasong He, E. van Ruymbeke, R. Keunings, and C. Baillya. Evaluation of different methods for the determination of the plateau modulus and the entanglement molecular weight. *Polymer*, 47:4461–4479, 2006.

[21] M. Doi and S.F. Edwards. Dynamics of concentrated polymer systems .3. Constitutive equation. *Journal of the Chemical Society - Faraday Transactions II*, 74:1818–1832, 1978.

[22] M. Doi. Molecular rheology of concentrated polymer systems 1. *Journal of Polymer Science: Polymer Physics Edition*, 18:1005–1020, 1980.

[23] R.P. Kusy and D.T. Turner. Dependence of fracture surface energy of PMMA on molecular weight. *Polymer*, 15:394–395, 1974.

[24] D.S.A. De Focatiis, C.P. Buckley, and Hutchings L.R. Roles of chain length, chain architecture, and time in the initiation of visible crazes in polystyrene. *Macromolecules*, 41:4484–4491, 2008.

[25] B.D. Lauterwasser and E.J. Kramer. Microscopic mechanisms and mechanics of craze growth and fracture. *Philosophical Magazine A*, 39(4):469–495, 1979.

[26] H.R. Brown. A molecular interpretation of the toughness of glassy polymers. *Macromolecules*, 24:2752–2756, 1991.

[27] H.R. Brown. Measurement of craze density by quantitative transmission electron microscopy. *Journal of Materials Science*, 14:237–239, 1979.

[28] N.J. Inkson, R.S. Graham, T.C.B. McLeish, D.J. Groves, and C.M. Fernyhough. Viscoelasticity of monodisperse comb polymer melts. *Macromolecules*, 39:4217–4227, 2006.

[29] L.L. Berger and E.J. Kramer. Chain disentanglement during high-temperature crazing of polystyrene. *Macromolecules*, 20:1980–1985, 1987.

[30] N. Tsuruta, T. Nakaoki, and H. Hayashi. A new method for determination of fibril volume fraction in polymer crazes by small-angle x-ray scattering. *Polymer Bulletin*, 39:201–208, 1997.

[31] R.P. Kambour. Measurement of craze density using optical techniques. *Nature*, page 1299, 1962.

[32] J.-H. Lin and A.C.M. Yang. Crazing micromechanism in glassy atactic polystyrene and its blends with poly(2,6-dimethyl-1,4-diphenyl oxides) by AFM. *Macromolecules*, 34:3698–3705, 2001.

[33] A.C.M. Yang, M.S. Kunz, and J.A. Logan. Micronecking operative during crazing in polymer glasses. *Macromolecules*, 26:1767–1773, 1993.

[34] E.J. Kramer and L.L. Berger. Fundamental processes of craze growth and fracture. *Advances in Polymer Science*, 91/92:1–68, 1990.

[35] A.V. Crewe and T. Groves. Thick specimens in the in the CEM and STEM i. Contrast. *Journal of Applied Physics*, 45:3662, 1974.

[36] A.C.M. Yang, E.J. Kramer, C.C. Kuo, and S.L. Phoenix. Crazes in diluted networks of polystyrene. *Macromolecules*, 19:2020–2027, 1986.

[37] J.S. Pedersen and P. Schurtenberger. Static properties of polystyrene in semidulute solutions: A comparison of Monte Carlo simulation and small-angle neutron scattering results. *Europhysics Letters*, 45(6):666–672, 1999.

[38] G. Binning, C.F. Quate, and Ch. Gerber. Atomic force microscope. *Physical Review Letters*, 56(9):930–933, 1986.

[39] D. Bonnell, editor. *Scanning Probe Micrscopy and Spectroscopy: Theory, Techniques and Applications. 2nd Ed.* Wiley-VCH Inc., 2001.

[40] L. Reimer. *Transmission Electron Microscopy: Second Edition.* Springer-Verlag, 1989.

[41] P.G. Klein, C.H. Adams, M.G. Brereton, M.E. Ries, T.M. Nicholson, L.R. Hutchings, and R.W. Richards. Rouse and reptation dynamics of linear polybutadiene chains studied by ^{2}H NMR transverse relaxation. *Macromolecules*, 31:8871, 1998.